Co-Transplantation-Based Human-Mouse Chimeric Brain Models to Study Human Glial-Glial and Glial-Neuronal Interactions

Mengmeng Jin[1,4], Ziyuan Ma[1,4], Haiwei Zhang[1,4], Ava V. Papetti[1], Rui Dang[1], Alessandro C. Stillitano[1], Steven A. Goldman[2,3], Peng Jiang[1,5]

[1]Department of Cell Biology and Neuroscience, Rutgers University, Piscataway, NJ 08854, USA.
[2]Center for Translational Neuromedicine, University of Rochester Medical Center, Rochester, NY, USA.
[3]Center for Translational Neuromedicine, University of Copenhagen Faculty of Health and Medical Sciences, Copenhagen, Denmark.
[4]These authors contributed equally
[5]Lead Contact

*Address correspondence to:
Peng Jiang, Ph.D.
Associate Professor
Department of Cell Biology and Neuroscience
Rutgers University
604 Allison Road, Piscataway, NJ 08854
Email: peng.jiang@rutgers.edu
Phone: 848-445-2805

Abstract

Human-mouse chimeric brain models, generated by transplanting human induced pluripotent stem cell (hiPSC)-derived neural cells, are valuable for studying the development and function of human neural cells in vivo. Understanding glial-glial and glial-neuronal interactions is essential for unraveling the complexities of brain function and developing treatments for neurological disorders. To explore these interactions between human neural cells within an intact brain environment, we employe a co-transplantation strategy involving the engraftment of hiPSC-derived neural progenitor cells along with primitive macrophage progenitors into the neonatal mouse brain. This approach creates human-mouse chimeric brains containing human microglia, macroglia (astroglia and oligodendroglia), and neurons. Using super-resolution imaging and 3D reconstruction techniques, we examine the dynamics between human neurons and glia, unveiling human microglia engulfing immature human neurons, microglia pruning synapses of human neurons, and significant interactions between human oligodendrocytes and neurons. Single-cell RNA sequencing analysis of the chimeric brain uncovers a close recapitulation of the human glial progenitor cell population, along with a dynamic stage in astroglial development that mirrors the processes found in the human brain. Furthermore, cell-cell communication analysis highlights significant neuronal-glial and glial-glial interactions, especially the interaction between adhesion molecules neurexins and neuroligins. This innovative co-transplantation model opens up new avenues for exploring the complex pathophysiological mechanisms underlying human neurological diseases. It holds particular promise for studying disorders where glial-neuronal interactions and non-cell-autonomous effects play crucial roles.

Introduction

While animal models have been invaluable in advancing our understanding of human brain development, aging, and the pathogenic mechanisms of neurological diseases [1-3], they may not fully recapitulate the cellular and molecular changes observed in the human brain, due to significant species-specific differences between humans and other model organisms. Limited availability of functional brain tissue from healthy individuals or patients with specific neurological disorders impedes our understanding of human brain development and aging, particularly in the context of disease. The emergence of human induced pluripotent stem cells (hiPSCs) presents new opportunities for overcoming these challenges [4]. Expanding on neural differentiation of hiPSCs, in vitro 2-dimensional (2D) human neural cell culture [5] and three-dimensional (3D) brain organoid models [6] have aided in uncovering mechanisms underlying human brain development and diseases [7,8]. Nevertheless, human iPSC-derived neural cells cultured in 2D, or 3D organoids often exhibit limited cellular and functional maturation and cellular heterogeneity [9,10]. Transplanting hiPSC-derived neural cells, such as dissociated human glial or neuronal cells [11-20], or intact cerebral organoids [21-25] into the brains of immunodeficient rodents to create chimeric brains can facilitate the improvement of cellular functionality and heterogeneity.

Cell-cell interactions, such as glial-neuronal and glial-glial interactions, are crucial for the proper functioning of the central nervous system (CNS). In the brain, microglia and macroglia, including astroglia and oligodendroglia, were historically perceived as support cells for neurons. However, recent research has illuminated their essential roles in regulating neuronal development and activity, synaptic transmission, and overall brain function [26]. Microglia, the brain-resident immune cells, engage in immune surveillance, inflammation, phagocytosis, regulating neurogenesis, and synaptic pruning - the removal of unnecessary synapses during development or in response to injury or disease [27]. Astroglia, the most abundant glial type, closely interact with neurons and synapses, modulating neuronal maturation and synaptic transmission [28]. Oligodendroglia are responsible for myelinating axons in the CNS, which greatly increases the speed and efficiency of neuronal communication. This myelination process is essential for proper neural signaling and is crucial for the function of the brain [29]. Understanding glial-neuronal and glial-glial interactions is vital for unraveling the complexities of brain function and developing therapeutic treatments for neurological disorders. In contrast to neurons, glial cells exhibit relatively lower evolutionary conservation, as evidenced by the limited ability of rodent glia to replicate the characteristics of human glia [12,30-35]. This underscores the necessity for employing species-specific tools to augment our understanding of human glial development, glial modulation of neuronal developmental and function, and glial-glial interactions. Various types of cells, such as human glial progenitor cells (GPCs), oligodendroglia progenitor cells (OPCs), immature astroglial cells, microglial progenitors (also known as primitive macrophage progenitors, PMPs), and neural progenitor cells (NPCs), have been utilized for solo cell type transplantation to establish human-mouse macroglial, microglial, or neuronal chimeric brains[11]. Human-mouse chimeric brains incorporate live human glia or neurons into the mouse brain, where they structurally and functionally integrate. However, the capacity of human-mouse chimeric brain models to explore human glial-neuronal and glial-glial interactions remains unexplored.

In this report, we present an innovative transplantation approach where NPCs and PMPs are co-transplanted into the brains of neonatal immunodeficient mice. Our findings reveal that the resulting chimeric mouse brains, which incorporate human microglia, astroglia, oligodendroglia, and neurons, provide a valuable model for studying the interactions between human neurons and glial cells. When brain organoids containing PMPs and ventralized NPCs were cultured under conditions conducive to glial formation, it was observed that human microglia could survive and functionally mature without the need for human colony-stimulating factor 1 (hCSF1) supplementation. This observation was corroborated by co-transplanting PMPs and ventralized NPCs into recipient mice without the requirement for a hCSF1 knock-in. Furthermore, single-cell RNA sequencing (scRNA-seq) of these co-transplanted chimeric brains identified diverse human cell types, various stages of astroglia

development, and the presence of human forebrain GPC populations, closely resembling those found in the human brain.

Results

Microglial-neuronal interactions in human-mouse chimeras containing human microglia, astroglia, and neurons (hMAN chimeric mice)

We aimed to establish a human-mouse chimeric brain model to investigate human glial-neuronal and glial-glial interactions. We derived PMPs and primitive NPCs (pNPCs) from control (Cont) hiPSC and human embryonic stem cell (hESC) lines that were fully characterized in our previous studies [14,36,37] (Figs. S1A-B). Most of the PMP cells expressed hematopoietic progenitor cell markers CD235 and CD43 (Figs. S1A-B), and nearly all pNPCs expressed SOX2 and PAX6 (Figs. S1A-B). Next, to further evaluate the identities of pNPCs and PMPs, we conducted RNA sequencing (RNA-seq). The results revealed distinct gene expression profiles for each cell type. Specifically, pNPCs exhibited high expression of NPC-associated genes such as SOX2, NES, and EOMES, while PMPs showed elevated expression of genes like CSF1R, SPI1, and C1QA, as illustrated in Fig. S1C. Moreover, the RNA-seq data for these pNPCs and PMPs showed no expression of pluripotent genes, such as NANOG and POU5F1 (Fig. S1D). Subsequently, PMPs and pNPCs at a 1-to-1 ratio were co-transplanted into the hippocampus of postnatal day 0 (P0) *Rag2*$^{-/-}$ *IL2rγ*$^{-/-}$ *hCSF1*^{KI} immunodeficient mice (Fig. 1A). At 7 months post-transplantation, xenografted cells labeled with the human-specific anti-nuclei antibody (hN) were primarily located in the cerebral cortex and hippocampus. Additionally, some of these cells had migrated and integrated with mouse cells at the periphery of the cluster of engrafted human cells (Fig. 1B, S1E). To determine the identity of hN$^+$ cells, we concentrated on examining the cells within the areas of the clusters of human cells (Fig. 1B3). We stained the brain sections prepared from 2 months and 7 months old mice with a neuronal marker NeuN, an astroglial marker GFAP, a microglia/macrophage marker IBA-1, and OLIG2, a marker for GPCs and oligodendroglial lineage cells (Figs. 1C, S1F). In 2-month-old chimeric brains, 57.5% of hN$^+$ cells expressed NeuN, 5.8% expressed IBA-1, 26.2% expressed OLIG2, and 10.3% expressed GFAP (Fig. S1G). We found that about 55.5% of the hN$^+$ cells expressed NeuN, 6.0% expressed IBA-1, 18.8% expressed OLIG2, and 19.3% of hN$^+$ cells expressed GFAP in 7 months old chimeric brains (Fig. 1D). To further assess the specific subtypes of neurons, we co-stained human-specific MAP2 (hMAP2) with glutaminase (GLS) or γ-aminobutyric acid (GABA), which is expressed in excitatory or inhibitory neurons [38] (Fig. 1E). As shown in Fig. 1F, there were 88.6% hMAP2$^+$/GLS$^+$ cells and 10.8% hMAP2$^+$/GABA$^+$ cells among the total hMAP2$^+$ human neurons, indicating that the engrafted human cells primarily differentiated into excitatory neurons.

To explore glial-neuronal interactions, we initially stained brain sections with human-specific antibodies recognizing TMEM119 (hTMEM119) and hMAP2 and observed that hTMEM119$^+$ microglia were positioned adjacent to hMAP2$^+$ neurons (Fig. 1G). Additionally, all hTMEM119$^+$ were positive for hN$^+$, confirming the presence of human microglia in this co-transplantation model (Fig. 1H). Microglia have been demonstrated to shape synaptic development, through engulfing and eliminating synapses [39]. Therefore, to investigate the function of synaptic pruning, we double-stained hTMEM119 with the human-specific pre-synaptic vesicle protein synaptophysin (hSyn) in brain sections prepared from 7-month-old chimeric mice. The 3D reconstruction images demonstrated that hSyn$^+$ puncta were colocalized within hTMEM119$^+$ microglia, indicating that these human synaptic proteins are phagocytosed by human microglia (Fig. 1I). In addition, to examine the phagocytosis of immature neurons by microglia, we co-transplanted GFP-labeled pNPCs and PMPs into the mouse brain. Then, we stained the brain sections prepared from 2-month-old chimeric mice with human-specific CD45 (hCD45) and intermediate progenitor stage marker TBR2 (Fig. 1J). Our findings revealed that hCD45$^+$ microglia phagocytized developing GFP$^+$TBR2$^+$ human neurons.

Using astroglial markers such as CD44 [40,41], GFAP, and S100B, we also examined the human astroglial population in the chimeric brain. The human astroglia labeled by human-specific CD44 (hCD44) developed complex structures with extended long, unbranched processes, as previously reported [34] (Fig. 1K). As shown in Fig. 1L, M, and S1H, we also observed that subpopulations of hCD44$^+$ cells that did not express GFAP (38.0% GFAP$^+$/hCD44$^+$ and 58.0% GFAP$^-$/hCD44$^+$ among the

total hCD44$^+$ cells) or S100B (59.8% S100B$^+$/hCD44$^+$ and 35.2% S100B$^-$/hCD44$^+$ among the total hCD44$^+$ cells). Since CD44 is also a marker for astroglial precursor cells [40], this suggests that these hCD44$^+$/GFAP$^-$ or hCD44$^+$/S100B$^-$ human astroglia were likely at immature stages. Additionally, in our 7-month-old chimeric brains, we did not find any hN$^+$ cells that expressed Octamer-binding transcription factor 4 (OCT4), a pluripotent stem cells marker and a tumor-initiating cells marker (Fig. S1I) [42,43]. In line with previous reports of sustained proliferation of human progenitor cells in chimeric brains [34,44], we also observed that a small population of hN$^+$ cells (1.8%) expressed the proliferation marker Ki67. Collectively, these results indicate that in the context of glial differentiation in a myelin-intact brain, the engrafted human pNPCs predominantly differentiated into astroglial cells, consistent with previous studies [45,46]. These findings demonstrate that the co-transplantation approach using hiPSC-derived pNPCs and PMPs effectively generates chimeric brains containing functional human microglia, macroglia, and neurons. This model is referred to as hMAN mice in this study.

Oligodendroglial-neuronal interactions in chimeric *shi/shi* × *Rag2*$^{-/-}$ mice containing human microglia, oligodendroglia, and neurons

By employing the same co-transplantation approach, we next aimed to create chimeric mouse brains containing human microglia, oligodendroglia, and neurons, referred to as hMON mice. We co-transplanted PMPs and pNPCs at a 1-to-1 ratio into the hippocampus of P0 shiverer (*shi/shi* × *Rag2*$^{-/-}$) immunodeficient mice (Fig. 2A). Shiverer mice, characterized by a mutation in the myelin basic protein (Mbp) gene [47,48], are commonly employed to investigate the myelination potential of transplanted cells [49,50]. The hypo-myelinated brain environment of shiverer mice facilitates the differentiation of transplanted cells into oligodendroglia. Furthermore, since shiverer mouse brains lack endogenous MBP expression, any detected MBP production is solely attributed to the xenografted cells [50]. As shown in Fig. 2B and S2A, the donor-derived hN$^+$ cells were distributed both in the cerebral cortex and hippocampus at 3 months post-transplantation. In our 4-month-old chimeras, we did not detect any hN$^+$ cells that expressed OCT4 (Fig. S2B), while approximately 17.3% of hN$^+$ cells expressed the proliferation marker Ki67 (Fig. S2C, S2D). To further explore the engrafted cell identity in shiverer mice, we also focused on examining the cells within the areas of the clusters of human cells (Fig. 2B3). We stained the mouse brain sections with NeuN, OLIG2, GFAP, IBA-1, and hN (Fig. 2C). We observed that approximately 57.6% of the hN+ cells expressed NeuN, 5.3% expressed IBA-1, 10.3% expressed GFAP, and a second large proportion, 25.7%, expressed OLIG2 (Fig. 2D). It is important to note that the shiverer mice were not humanized for CSF1, suggesting that the co-transplantation approach was sufficient to support the survival of human microglia. To further validate whether this approach could support human microglia survival in different mouse strains, we transplanted the same combination of pNPCs and PMPs into *Rag1*$^{-/-}$ mice. We stained the mouse brain sections and observed the presence of NeuN$^+$/hN$^+$, GFAP$^+$/hN$^+$, OLIG2$^+$/hN$^+$ cells, and particularly IBA-1$^+$/hN$^+$ human microglia (Fig. S2E). The presence of human microglia cells in *Rag1*$^{-/-}$ mice was further confirmed by the detection of cells positive for human-specific CD45 (hCD45) (Fig. S2F).

To further examine the oligodendroglial population, we co-stained hN with NG2, a marker for OPCs, or MBP, a marker for mature oligodendrocytes (Figs. 2E-G). We found a large number of hN$^+$/NG2$^+$ cells and a few MBP$^+$ cells in the hMON chimeric mice at three months post-transplantation (Figs. 2E-G). As shown in Fig. 2G, the 3D reconstruction images demonstrated soma and cytoplasmic processes of MBP$^+$ oligodendrocytes. This suggests that engrafted human pNPCs differentiation into NG2$^+$ OPCs that began to mature into myelinating oligodendrocytes at three months post-transplantation. To further investigate the interactions of oligodendrocytes and neurons, we performed co-staining for MBP and hMAP2. The 3D reconstruction images demonstrated that MBP$^+$ oligodendrocytes began to form myelinating contacts with hMAP2$^+$ human neurons (Fig. 2G). By examining the staining from *Rag2*$^{-/-}$ *IL2rγ*$^{-/-}$ *hCSF1*^{KI} and shiverer mice with human-specific NG2 (hNG2), we observed a higher abundance of hNG2$^+$ OPCs in shiverer mice compared to *Rag2*$^{-/-}$ *IL2rγ*$^{-/-}$ *hCSF1*^{KI} mice (Fig. 2H, 2I). In addition, to further explore the specific subtypes of neurons, we co-stained hMAP2 with GABA and observed the presence of hMAP2$^+$GABA$^+$ inhibitory neurons (Figs.

S2G, S2H). Taken together, these findings demonstrate that the co-transplantation approach enables the creation of hMON chimeric brains containing functional human microglia, oligodendroglia, and neurons, without the need for a human CSF1 knock-in in the host transgenic mice.

Co-transplantation of PMPs and ventralized NPCs to generate chimeric brains

Microglia rely on signals from the colony stimulating factor-1 receptor (CSF1R) for survival, proliferation, and differentiation, which are activated by either CSF1 or interleukin-34 (IL-34) [51]. Previous studies have shown that microglia cannot survive in dorsal forebrain organoids without the addition of these survival factors [24]. In the developing brain, CSF1 is mainly produced by glial cells, especially astroglial cells [52,53]. Therefore, we hypothesized that culturing organoids under gliogenic conditions might obviate the need to add CSF1 or IL-34 to the culture. We first obtained partially ventralized NPCs (v-NPCs) by treating pNPCs with purmorphamine (Pur), a small-molecule agonist of the Sonic Hedgehog (SHH) signaling pathway, for one week [54]. After one week of patterning, 30.2% of NPCs expressed the dorsal brain marker PAX6, 35.1% expressed the ventral prosencephalic progenitor marker NKX2.1, and 7.5% were OLIG2$^+$ (Fig. S3A). As shown in Fig. 3A, we then co-cultured these v-NPCs and PMPs at a ratio of 1:1 in 3D to generate microglia-containing brain organoids, using a procedure described in our previous study [8]. As reported recently [25], we cultured the organoids in a medium containing the gliogenic agent PDGF-AA from day 4 to 18, after which we switched to a neuronal differentiation medium for continued culture till day 32. Throughout the culture period, no CSF1 or IL-34 was supplemented (Fig. 3A).

To explore the survival and maturation of PMPs into microglia in these brain organoids, we examined the expression of microglial markers at day 9 and day 30. At day 9, 4.2% of cells expressed CD45 and 2.8% expressed PU.1, a transcription factor essential for microglial differentiation (Fig. 3B and C) [55]. Next, we examined the identity of microglia at the neuronal differentiation stage using the homeostatic microglia marker TMEM119. At day 30, there were cells expressing CD45 (Fig. 3D), and about 13.88% of cells expressing hTMEM119 in the organoids (Fig. 3E and H). To investigate the neuronal and astroglial differentiation in the brain organoids, we stained these organoids with GABA, TUJ-1, and S100B. Due to the patterning of pNPCs to NKX2.1$^+$ ventral neural progenitors, we observed 10.28% GABA$^+$/TUJ-1$^+$ inhibitory neurons (Fig. 3F, H). S100B$^+$ astroglia accounted for 12.34% of the total cells (Fig. 3G, H). High levels of CSF1, IL34, and IBA-1 gene expression were detected in our day 14 organoids, whereas these genes could not be detected in undifferentiated pNPCs (Fig. 3I). Furthermore, microglia have been shown to engulf neural progenitors in organoids [8,56,57]. The 3D reconstruction of hTMEM119 with SOX2 staining images demonstrated that SOX2$^+$ cells were colocalized within hTMEM119$^+$ microglia, indicating that these microglia were functional and phagocytized NPCs (Fig. 3E). These observations confirm that PMPs were likely supported by CSF1 and IL-34 produced by neural lineage cells in the organoids and further differentiated into microglia.

To further explore the differentiation of human PMPs into microglia independently of human CSF1 knockin *in vivo*, we co-transplanted v-NPCs and PMPs into *Rag2*$^{-/-}$ immunodeficient mice (Fig. 3J). We observed the hN$^+$ cells expressing IBA-1, along with hN$^+$/GFAP$^+$, hN$^+$/OLIG2$^+$ (Fig. 3I), and hN$^+$/GABA$^+$ cells (Fig. S3B) in the *Rag2*$^{-/-}$ mouse brain. These findings collectively confirm that PMPs differentiate into microglia both in our brain organoids without the addition of CSF1 or IL-34 and in chimeric mouse brains independently of CSF1 knockin in the host mice.

scRNA-seq of hMAN chimeric mouse brains reveals heterogeneous glial populations and robust cell-cell interactions

To explore the transcriptional characteristics of co-transplanted cells, we conducted scRNA-seq on the brains of 3-month-old *Rag2*$^{-/-}$ *IL2rγ*$^{-/-}$ *hCSF1*^{KI} mice, which had been co-transplanted with human pNPCs and PMPs. We collected 23,994 high-quality human cells from the chimeric mouse brain after quality control and filtration (Figs. 4A, S4A). Subsequent dimensional reduction and cluster analysis revealed 19 clusters (Figs. S4B, S4C) representing 8 major human cell types (Fig. 4B): radial glia, NPCs, excitatory neurons, inhibitory neurons, GPCs, astrocytes, microglia, and vascular

leptomeningeal cells (VLMCs). Cell cycle regression analysis identified three radial glial clusters and one NPC cluster with a high proportion of cells in the cell cycle (Fig. S4D). These cells express proliferation markers but lack pluripotency markers (Fig. S4E). Additionally, copy number variation (CNV) analysis revealed no genomic alterations in the transplanted human cells (Fig. S4F), further excluding the tumorigenic potential of these cells. Similarity analysis with human pre- and post-natal brain samples [58] indicated that the human cells approximated a developmental stage matching the late second trimester of human brain tissue three months post-transplantation, and the transplanted cells exhibited a similar predicted developmental age to that of human brain organoids transplanted into rodent brains for 5 and 8 months [23,25] (Fig. S4G). We identified a distinct cell population characterized by high expression of *EGFR*, *OLIG1*, and *OLIG2* genes, but with limited expression of OPC markers (*PDGFRA*, *CSPG4*, *PCDH15*), oligodendrocyte markers (*MBP*, *CTNNA3*, *FOXO4*), and astrocyte markers (*GFAP*, *S100B*, *SLC6A11*) (Fig. 4C). Jaccard similarity analysis suggested that these cells share transcriptomic signatures with glial progenitors identified in cortical macroglial cells from human brain tissue and show low similarity with astroglia and oligodendroglia [59] (Fig. 4D). Consequently, we classified these cells as human GPCs. To further validate this identity, we performed immunostaining for *ETV4*, a recently identified GPC marker [60], and observed the presence of both $hN^+/ETV4^+$ cells (Fig. 4E). In addition, we also found $hNG2^+/ETV4^+$(Fig. S4H), aligning with the scRNA-seq findings (Fig. 4C). However, we did not observe a high THY1 expression in our GPC population, as stated in Liu et al.[60] (Fig. S4I). In addition, we dissected the astroglial populations, identifying five distinct stages of astroglial development (Fig. 4F). Pseudotime analysis suggested that clusters Astro 2 and Astro 3 represented more advanced stages of astroglial maturity (Fig. 4G), with Astro 3 characterized as a protoplasmic astroglial subtype ($GFAP^-/SLC1A3^+$), and Astro 2 as a mature fibrous astroglial subtype ($GFAP^+/SLC1A3^-$, Fig. 4H) [59]. Moreover, Astro 1 and Astro 4 clusters shared gene expression signatures with astroglial progenitor cells from the human hippocampus [61] (Fig. 4I). Notably, these astroglial stages did not align with signatures associated with cell death (AST3 in Fig. 4I), further indicating their alignment with early developmental stages of the human brain.

The presence of both human neurons and diverse glial populations in chimeric brains offers a fresh avenue for scrutinizing their specific ligand-receptor interactions via cell-cell communication (CCC) analysis of scRNA-seq data (Fig. 4J). Regarding neuronal-glial interactions, inferred ligand-receptor pairs (Fig. 4K, S4J) could be sorted into distinct signaling pathways (Fig. 4K). This analysis pinpointed several crucial pathways implicated in neuronal-glial interactions, including the amyloid precursor protein (APP), pleiotrophin (PTN), midkine (MK), and neurexin (NRXN) signaling pathways. Notably, the APP signaling pathway exhibited the highest signaling probability between microglia and neurons (Fig. 4L). These findings hold high relevance, as the APP pathway is recognized for its role in regulating microglia phenotypes [62]. Communication within the NRXN signaling pathway was notably enriched between neurons and astroglia (Fig. 4M). Interactions between NRXN-calsyntenin (CLSTN) play pivotal roles in excitatory and inhibitory synaptogenesis during development [63-65], and NRXNs and neuroligins (NLGNs) constitute a critical pair of synaptic adhesion molecules crucial for synapse development and function [66]. These findings underscore that the hMAN model faithfully mirrors human neuro-glial interactions.

Next, we explored glial-glial interactions (Figs. 4N, S4K). The SPP1 (secreted phosphoprotein 1, osteopontin) signaling pathway was detected within the microglial population and between microglia and astroglia (Fig. 4N). This aligns with previous studies indicating that SPP1 signaling fosters microglial growth and synaptic pruning during development [67]. Additionally, it facilitates interactions between microglia and astroglia, promoting astrogliosis and migration [67]. We also noted the presence of the pleiotrophin (PTN) signaling pathway within and between astroglial and GPC interactions (Fig. 4O). Astroglia were found to have significant roles in the PTN signaling pathway and serve as key recipients in the midkine (MK) signaling pathway (Fig. 4O), both of which are heparin-binding cytokines associated with differentiation and growth[68-70] . PTN also acts as an angiogenesis factor [71], elucidating the observed correlation with angiogenic astroglial subtypes in the human brain (Fig. 4I) and robust PTN signaling within astroglia (Fig. 4O). Furthermore, PTN/MK signaling pathways between astrocytes

and neurons (Fig. 4K) suggest crucial roles of astroglia in neurogenesis and neurite growth [72,73]. A recent preprint has also underscored the importance of astrocyte-secreted PTN in maintaining neuronal dendrite morphology and synaptic circuitry during normal and Down syndrome brain development [74].

GPCs play a predominant role in the NOTCH signaling pathway among all other cell types (Fig. 4P). This pathway is crucial for gliogenesis and specifying cell fate [75]. We observed that the delta (DLL) signals from neurons interact with NOTCH receptors from both GPCs and astrocytes. Similarly, GPC-secreted DLL or Jagged (JAG) signals interact with astrocytes and other GPCs through the NOTCH signaling pathway. This finding aligns with previous knowledge that Delta-NOTCH signaling directs neuron and glial differentiation [76]. Furthermore, we found that macroglial NOTCH activation by Jagged (JAG) ligands from all glial cell types underscores the importance of JAG-NOTCH signaling in maintaining a proliferative glial pool [77]. Notably, we observed specific NRXN1-NLGN3 signaling pathway interactions within the astroglial population, highlighting the importance of this pathway in controlling astroglial morphogenesis, synaptogenesis, and synaptic functions [78]. Taken together, our scRNA-seq data from the hMAN chimeric brain revealed the presence of newly characterized human forebrain GPC cell type [60], identified dynamic astroglial subpopulations, and recapitulated critical signaling pathways between cell types during brain development.

Discussion

Previous studies have shown that mouse brains possess the ability to incorporate live human glial cells or neurons. These human cells can structurally and functionally integrate into the mouse brain, where they widely disperse, establish connections, and interact dynamically with the host murine brain cells, creating human-mouse chimeric brains [11]. In this study, we further demonstrate that by co-transplanting hPSC-derived PMPs and pNPCs, we can generate human-mouse chimeric brains that incorporate human microglia, macroglia, and neurons. Earlier research has indicated that engrafted PDGFRα-expressing human OPCs differentiate into astroglia or oligodendroglia, depending on the brain environment. In a hypomyelinated context, using immunodeficient shiverer mice as hosts, human OPCs predominantly differentiate towards oligodendroglia [44,79,80]. Conversely, in myelin-intact immunodeficient mice, OPCs tend to differentiate more towards astroglia [17,34,44]. Consistent with these findings, we also observe that engrafted human pNPCs respond to the brain environment, primarily generating astroglial lineage cells in myelin-intact brains while developing into oligodendroglial lineage cells in myelin-deficient brains. The distribution of human cells in the hMAN and hMON models differs from that in glial chimeras, where donor-derived human macroglia[34,79] or microglia [13,81-83] uniformly and widely colonize the host tissue. This difference is likely attributable to the varying migration capabilities between neurons and glial cells in the postnatal brain[84], as well as the specific injection sites we targeted. Post-transplantation, these pNPCs efficiently differentiate to neurons which typically exhibit less migratory tendencies compared to OPCs or microglia. Additionally, targeting the hippocampal formation or the cerebral cortex[19,85] may result in less dispersal compared to targeting locations such as the lateral ventricle [18,36,86]. While some cells migrate and integrate with mouse cells at the periphery of the human cell clusters, the majority of the cells form structures, resembling implant organoids in appearance [23-25,87]. Importantly, the human microglia differentiated from co-transplanted PMPs colocalize with human neurons and macroglia. These human glia and neurons actively interact with each other in the hMAN and hMON chimeric mice.

In addition to creating chimeric mouse brains with various human neural cell types, another significant benefit of conducting co-transplantation is avoiding the necessity of using human CSF1 or IL-34 knockin mice[81,88]. The sustained survival of hPSC-derived microglia within the mouse brain requires transgenic expression of human CSF1 or IL-34 because previous studies have demonstrated that no human microglia survive when human *CSF1* is replaced with murine *Csf1* [81]. A recent study showed that transplanting intact cerebral organoids containing microglial progenitors can lead to the development of human microglia in vivo in host mice that are not humanized for CSF1, owing to the release of human CSF1 and IL-34 by the neural lineage cells in the organoids[24]. Consistently, we show that when PMPs are co-transplanted with dissociated pNPCs, these PMPs also survive and differentiate into human microglia in chimeric mouse brains. Notably, in in vitro culture, the neural lineage cells in dorsal forebrain brain organoids are unable to release sufficient human CSF1 and IL-34 to support human microglia differentiation [24]. To further improve microglia-containing brain organoid models, we discover that generating organoids with ventralized NPCs and further culturing under gliogenic culture conditions can eliminate the need for adding IL-34 or CSF1 to the culture. Previous studies have demonstrated the production of IL-34 and CSF1 from glial cells, particularly astroglial cells [52,53]. We have also observed robust expression of IL-34 and CSF1 in these organoids, which may explain why PMPs within these organoids can mature into microglia with phagocytic functions successfully. This new organoid model has the potential to significantly reduce the high cost associated with the long-term culture of microglia-containing organoids. As anticipated, when PMPs and ventralized NPCs are co-transplanted into *Rag2*$^{-/-}$ immunodeficient mice, we observe human microglia, macroglia, and neurons, especially GABA^{+} inhibitory neurons in chimeric brains, providing opportunities to explore the interactions of human microglia with human interneurons.

The presence of bipotent GPCs in the developing human forebrain, capable of differentiating exclusively into oligodendroglia and astroglia, has long been a topic of speculation and discussion. As opposed to mouse brain development, human brain development is a prolonged process, which likely

offers wide time windows and greater opportunities to capture the GPC population. Indeed, recent studies employing single-cell RNA-seq [89] and advanced flow cytometry with sophisticated cell-surface markers [60] have conclusively demonstrated the presence of GPCs in the developing human forebrain. Consequently, creating experimental models of human forebrain GPCs would be instrumental in understanding human glial development, function, and heterogeneity under normal and disease conditions, including neurodegeneration and gliomagenesis [90,91]. While hPSCs present significant potential for developing such models, recapturing human forebrain GPCs through neural differentiation of hPSCs has proven difficult. In 2D cultures, deriving human GPCs requires retinoic acid treatment and activation of sonic hedgehog signaling, causing human cells to adopt ventral spinal cord identities [79,92]. These GPCs with spinal cord identities are likely not equivalent to human GPCs with forebrain identities, considering that glial cells originating from different brain regions during development exhibit distinct gene expression profiles and functional characteristics[93,94]. Partly because of the delayed onset of cortical gliogenesis, replicating glial cell development and heterogeneity in 3D forebrain organoids in vitro is challenging, and the detection of GPCs is seldom reported [25,95]. While transplantation of intact organoids into rodent brains has enhanced glial development [25,96], recent studies primarily documented astroglial lineage cells, such as NFIA-expressing cells [25]. In our hMAN mice, we present the following evidence demonstrating the generation of forebrain human GPCs from engrafted PAX6$^+$ dorsal forebrain pNPCs: 1) scRNA-seq data revealed a glial population characterized by high expression of *EGFR*, *OLIG1*, and *OLIG2*, but low levels of astroglial and oligodendroglial markers; 2) Comparative analysis with macroglial cells isolated from human brain tissue indicated that this cluster exhibits high transcriptomic similarity to human glial progenitors; and 3) Immunostaining of the hMAN chimeric brain confirmed the presence of ETV4, a newly identified marker for GPCs, in human cells. In addition, in comparison to the transplantation of intact organoids into the mouse brain [25], engrafting dissociated human neural cells may also promote the diversification of human astroglia. In our hMAN brain, we observed significant heterogeneity among human astroglia. We identified five distinct astroglial subclusters exhibiting dynamic transcriptomic profiles, including GFAP$^+$ fibrous astrocytes and GLAST+ protoplasmic astrocytes. Additionally, we identified a subpopulation of astrocyte progenitor cells by comparing them with astrocytes isolated from human brains at early developmental stages. Some subpopulations of astrocytes exhibit angiogenic features similar to those of human astrocytes, which correlates with the pro-angiogenic effects of the PTN signaling pathway predicted from our cell-cell interaction analysis.

The hMAN and hMON chimeric models present new avenues for investigating interactions between human neurons and glia in vivo under both neurodevelopmental and neurodegenerative conditions. Our scRNA-seq analysis of hMAN mouse brains uncovers the intricate ligand-receptor interactions between human neuron-astroglia and astroglia-astroglia, highlighting the significant role of NRXN-NLGN signaling pathways. This aligns with recent reports analyzing RNA-seq datasets from GPCs isolated from human brain tissue [97], and single-cell datasets from the developing human fetal cortex and examining astroglial differentiation in cerebral organoids[98]. NRXN-NLGN has been shown to serve as a crucial ligand-receptor pair driving human astroglia development [98]. Additionally, studies in mice indicate that NLGN and NRXN play essential roles in neuronal spinogenesis, synaptic formation, and astrocyte morphogenesis [66,78]. There are multiple members in the NRXN and NLGN families [99,100]. Our cell-cell interaction analysis reveals the crucial involvement of NRXN1-NLGN3 in both neuron-astroglia and astroglia-astroglia interactions. This aligns with previous findings that in human astrocytes, the mRNA level of NLGN3 is higher than that of NLGN1 and NLGN2, and NRXN1 is higher than NRXN2 and NRXN3 [101]. Notably, a mutation of the arginine-451 to cysteine in the NLGN3 gene (NLGN3 R451C mutation) has been associated with susceptibility to autism and Asperger syndrome [102]. Previous studies using transgenic mice and hiPSCs have predominantly focused on the impact of NLGN3 R451C on neuronal functions and show gain-of-function effects, such as enhanced excitatory synaptic strengths in neurons with NLGN3 R451C [103,104]. Our findings of the involvement of NRXN1-NLGN3 in astroglia-astroglia interactions underscore the importance of exploring not only neuronal

functions but also astroglia-astroglia interactions. Given the high heterogeneity of human astroglia and robust cell-cell connections in hMAN mice, this model provides a valuable tool for studying how changes in cell adhesion molecules, such as the autism-linked NLGN3 R451C, impact neuronal-astroglial, and astroglial-astroglial interactions. Additionally, recent research has highlighted microglial dysfunction as a central mechanism in Alzheimer's disease (AD) etiology [30,105,106]. Co-transplantation of PMPs and pNPCs from early-onset AD iPSCs, such as Down syndrome iPSCs [107,108] or Tau 4R iPSCs [109], capable of generating Aβ and/or tau pathologies, to develop hMAN and hMON mice could expose human microglia and macroglia to a brain environment with both intracellular and extracellular pathological Aβ and/or hyperphosphorylated tau proteins. With human microglial-neuronal and microglial-oligodendroglial interactions detected in hMAN and hMON respectively, these models also offer new opportunities to better understand mechanisms mediated by human microglia in the pathogenesis of AD.

Acknowledgments

This work was in part supported by grants from the NIH (R01NS102382, R01NS122108, and R01AG073779 to P.J.). M.J. was supported by a postdoctoral fellowship award from the New Jersey Department of Health (CAUT24DFP004). A.V.P. was supported by a graduate trainee T32 fellowship award from the Training in Translating Neuroscience to Therapies program at Rutgers University (T32NS115700). We appreciate Dr. James Knowles from Rutgers University for aiding in library preparation for scRNA-seq. We are thankful to Mr. Kushal Aluru and Ms. Rachael Kim from the Jiang laboratory for their assistance with immunohistochemistry.

Author Contributions

M.J. and P.J. designed experiments and interpreted data; M.J. and H.Z. carried out most of the experiments with technical assistance from Z.M., A.S., and R.D.; Z.M. performed RNA-seq data analyses and assisted with sequencing data interpretation; A.V.P. conducted brain organoids culture. S.G. provided critical suggestions to the overall research direction and the immunodeficient shiverer mouse model; P.J. conceived the concepts, directed the project, and wrote the manuscript together with M.J., Z.M., and input from all co-authors.

Competing Financial Interests

The authors declare no competing financial interests.

Methods

Human iPSC and hESC lines generation and culture

One control hiPSC line and one control hESC line were used in this study. The hiPSCs and hESCs were cultured on dishes coated with hESC-qualified Matrigel (Corning) in mTeSR Plus medium (STEMCELL Technologies) under feeder-free conditions. Both hiPSCs and hESCs were passaged once per week using the ReLeSR medium (STEMCELL Technologies).

Animals

All animal work was conducted without gender bias with the approval of the Rutgers University Institutional Animal Care and Use Committee. The animals used in this study were as follows: B6.129S6-*Rag2*$^{-/-}$ (The Jackson Laboratory; 008449), B6.129S7-*Rag1*$^{-/-}$ (The Jackson Laboratory; 002216), *Rag2*$^{-/-}$ *IL2rγ*$^{-/-}$ *hCSF1*^{KI} (The Jackson Laboratory; 017708), and *shi/shi x Rag2*$^{-/-}$ (generated by Dr. Steven Goldman group at University of Rochester).

Differentiation and culture of PMPs, pNPCs, and NPCs

PMPs were generated from the control hiPSC and hESC lines using a previously established protocol [13,14,110,111]. Yolk sac embryoid bodies (YS-EBs) were generated by treating them with mTeSR 1 medium (STEMCELL Technologies) supplemented with bone morphogenetic protein 4 (BMP4, 50 ng/ml), vascular endothelial growth factor (VEGF, 50 ng/ml), and stem cell factor (SCF, 20 ng/ml) for 6 days. To induce myeloid differentiation, the YS-EBs were plated on dishes with X-VIVO 15 medium (Lonza) supplemented with interleukin-3 (IL-3, 25 ng/ml) and macrophage colony-stimulating factor (M-CSF, 100 ng/ml). Four to six weeks after plating, human PMPs emerged in the supernatant and continued to be produced for more than three months.

Human pNPCs were generated from hiPSCs and hESCs [45]. The pNPCs were cultured in a medium consisting of a 1:1 mixture of Neurobasal (Thermo Fisher Scientific) plus GlutaMax (Gibco) and DMEM/F12 (Hyclone), supplemented with 1x N2, 1x B27-RA (Thermo Fisher Scientific), FGF2 (20 ng/ml, Peprotech), CHIR99021 (3 µM, Biogems), human leukemia inhibitory factor (hLIF, 10 ng/ml, Millipore), SB431542 (2 µM), and ROCK inhibitor Y-27632 (10 µM, Tocris). The pNPCs were passaged with TrypLE Express (Thermo Fisher Scientific) once per week. pNPCs within 6 passages were used for organoid generation.

To obtain ventralized NPCs, the expanded pNPCs were dissociated into single cells using TrypLE Express (Thermo Fisher Scientific). Next, the pNPCs were cultured in suspension in the presence of ROCK inhibitor Y-27632 (10 µM) at the first day in ultra-low-attachment 6-well plates. To pattern these neurospheres towards a ventral forebrain fate, we treated them with purmorphamine (1 µM, Cayman Chem), an agonist of sonic hedgehog signal pathway for one week (Figure 1A). The media were replenished every day. After one week of patterning, the neurospheres were dissociated into single cells using TrypLE Express. Then, the NPCs were cultured in a medium consisting of a 1:1 mixture of Neurobasal (Thermo Fisher Scientific) and DMEM/F12 (Hyclone), supplemented with 1x N2, 1x B27-RA (Thermo Fisher Scientific), FGF2 (20 ng/ml, Peprotech), and ROCK inhibitor Y-27632.

Brain organoid culture

The brain organoids were generated from a total of 10,000 cells (5,000 NPCs and 5,000 PMPs), in each well of ultra-low-attachment 96-well plates in the presence of ROCK inhibitor Y-27632 (10 mM) [8]. The culture medium was composed of a 1:1 mixture of PMP medium and NPC medium (1:1 mixture of Neurobasal and DMEM/F12, supplemented with 1x N2 (Thermo Fisher Scientific), 1x B27-RA (Thermo Fisher Scientific), and FGF2 (20 ng/ml, Peprotech) for four days (day 4). Then, the organoids were transferred to ultra-low-attachment 6-well plates and cultured with gliogenic medium which was composed of DMEM/F12, supplemented with 1x N2, FGF2 (10 ng/ml), PDGF-AA (10 ng/ml, Peprotech), IGF1 (10 ng/ml, Peprotech), and dibutyryl-cyclic AMP (1 uM, Sigma) for two weeks (day 18). The medium was replenished every two days, and starting from day 4, the cell culture plates were kept on

an orbital shaker at a speed of 85 rpm. To promote neural differentiation, organoids were cultured in differentiation media, comprised of a 1:1 mixture of Neurobasal and DMEM/F12, supplemented with 1x N2, BDNF (10 ng/ml, Peprotech), GDNF (10 ng/ml, Peprotech), dibutyryl-cyclic AMP (1 uM), and ascorbic acid (200 nM, Sigma), from day 18 onwards.

Cell transplantation

PMPs and pNPCs or v-NPCs were collected from the supernatant and suspended at a concentration of 100,000 cells/µl in PBS. Cells were then injected into the brains of P0 B6.129S7-*Rag1*$^{-/-}$, B6.129S6-*Rag2*$^{-/-}$, *Rag2*$^{-/-}$ IL2rγ$^{-/-}$ *hCSF1*^{KI}, and *shi/shi x Rag2*$^{-/-}$ immunodeficient mice. The transplantation sites were bilateral from the midline = ±1.0 mm, posterior from bregma = −2.0 mm, and dorsoventral depths = −1.5 and −1.2 mm. The pups were placed in ice for 4-5 mins to anesthetize and then injected with 0.5 µl of cells into each site (four sites total) using a digital stereotaxic device (David KOPF Instruments) that was equipped with a neonatal mouse adapter (Stoelting).

Tissue immunostaining, image acquisition, and analysis

Mouse brains were fixed in 4% paraformaldehyde and subsequently dehydrated by immersion in 20% and then 30% sucrose solutions. Brain organoids were fixed in 4% paraformaldehyde for 2 hours then dehydrated by immersion in a 25% sucrose solution. Following dehydration, brain tissues and organoids were embedded in the OCT compound and frozen for sectioning. Cryosections with a thickness of 30 µm were obtained from mouse brains and with a thickness of 12 µm from brain organoids for immunofluorescence staining. For immunostaining, tissue sections were first blocked with a solution containing 5% goat serum in PBS with 0.8% Triton X-100 at room temperature for 1 hour; brain organoids were blocked with a solution containing 5% goat serum in PBS with 0.2% Triton X-100. Primary antibodies (listed in Supplementary Table 1) were diluted in the blocking solution and incubated with the tissues overnight at 4°C. After primary antibody incubation, sections were washed with PBS and then incubated with secondary antibodies for 1 hour at room temperature. After immunostaining, 7-month-old brain sections were performed with TrueBlack treatment as previously described [110]. Following another round of PBS washing, slides were mounted with anti-fade Fluoromount-G medium containing DAPI (1,4,6-diamidino-2-phenylindole dihydrochloride) from Southern Biotechnology. Fluorescent images were captured using a Zeiss 800 confocal microscope and the all-in-one fluorescence microscope BZ-x800 (Keyence).

Large scale images in Fig. 1B, S1E, 2B, and S2A were obtained by confocal tile scan by the Keyence BZ-x800 software. To obtain a 3D reconstruction, images were processed by the Zen software (Zeiss). To visualize phagocytic function, super-resolution images in Figures. 1 and 3 were acquired by Zeiss Airyscan super-resolution microscope at 63X with 0.2mm z-steps. To generate 3D-surface rendered images, super-resolution images were processed by Imaris software (Bitplane 9.9).

RNA isolation and quantitative reverse transcription PCR

RNA extraction was done by the Qiagen Mini kit (Qiagen: 74104) and Qiagen shredder (Qiagen: 79656). Reverse transcription was also done with SuperScript™ IV VILO™ Master Mix (Thermo Fisher Scientific: 11756050). Real-time PCR was performed on the ABI 7500 Real-Time PCR System using the TaqMan Fast Advanced Master Mix (Thermo Fisher Scientific). All primers are listed in Supplementary Table S2. The $2^{-\Delta\Delta Ct}$ method was used to calculate relative gene expression after normalization to the GAPDH internal control.

Bulk RNA sequencing library preparation and data analysis

Libraries for bulk RNA-seq were prepared using the Illumina TruSeqV2 kit (Illumina, San Diego, CA) following the manufacturer's protocol. Sequencing was performed on a Novaseq X Plus with 150 bp paired-end reads. The sequenced reads were quality-checked with FastQC (v0.12.1) and trimmed for adaptor and low-quality sequences using Trim Galore (v0.6.10). Trimmed reads were mapped to the GRCh38 reference genome and GENCODE v44 primary assembly using STAR[112] (v2.7.11a). Read

count extraction and normalization were performed with RSEM[113] (v1.3.1), and differential expression analysis (DEG) was conducted using the DESeq2[114] R package (v1.42.0). Heatmaps were generated using the pheatmap R package (v1.0.12).

Single-cell RNA sequencing library preparation

Two hMAN *Rag2*$^{-/-}$ *IL2rγ*$^{-/-}$ *hCSF1*^{KI} chimeric mice were anesthetized and perfused with cold 1x Dulbecco's Phosphate-Buffered Saline (DPBS). Brains were then dissected and dissociated using the Adult Brain Dissociation Kit (Miltenyi Biotec) according to the manufacturer's instructions. Human cells were isolated using the Mouse Cell Depletion Kit (Miltenyi Biotec), following the manufacturer's protocols. The isolated cell suspension from the two mice were subsequently loaded into the Chromium Controller respectively for single-cell RNA sequencing (scRNA-seq) library preparation, utilizing the Chromium Next GEM Single Cell 3' Kit v3.1 and Dual Index Kit TT Set A, in accordance with the manufacturer's guidelines. Quality control of the scRNA-seq libraries was performed using an Agilent 2100 Bioanalyzer, and the libraries were sequenced on a NovaSeq 6000 system using S4 flow cells.

Single-cell RNA sequencing data analysis

Raw reads were mapped to the human (GRCh38, Ensembl 98, GENCODE v32) and mouse (mm10, Ensembl 98, GENCODE vM23) reference genomes using Cell Ranger (v7.1.0), with the EGFP sequence included. Cells were classified as human if more than 95% of the reads mapped to the human reference genome. Filtered human cells were retained for further analysis if they contained between 1,000 and 5,000 genes, had fewer than 30,000 unique molecular identifiers (UMIs), and exhibited mitochondrial content below 15%. Doublets and multiplets were removed using the scDblFinder R package [115].

Downstream analysis was conducted using the Seurat R package (v5.0.3) [109]. Raw gene count matrices were normalized by regularized negative binomial regression using the *SCTransform()* function (vst.flavor = "v2"), which also identified the top 3,000 highly variable genes using default parameters. Dimensionality reduction was performed using principal component analysis (PCA) on the top variable genes. Clusters of cells were identified in PCA space through shared nearest-neighbor graph construction and modularity detection, implemented by the *FindNeighbors()* and *FindClusters()* functions, using a dataset dimension of 50 and a resolution parameter set to 0.5. Astrocyte subclusters were identified by first isolating the astrocyte cells (n = 11,100) from the complete dataset. These cells were then processed using the SCTransform method, followed by dimensionality reduction (npcs = 50, ndims = 30). Clustering was subsequently performed with a resolution parameter set to 0.2.

For age prediction, we employed Seurat's reference mapping method by projecting our data and the organoid data [25] onto the brain age reference dataset [58]. The predicted age distribution before birth among different groups was compared using the paired Wilcoxon rank-sum test after randomly subsetting 100 cells per group. The Jaccard similarity index was calculated using the GeneOverlap R package (v1.38.0), with similarity significance calculated from Fisher's exact test. Pseudotime analysis was performed using the monocle3 R package (v1.3.4) [116-118] with default parameters. The root cell type for the start of the trajectory was chosen manually by finding an endpoint in the astrocyte progenitor population in cluster Astro 1. To study cell-cell communication between transplanted human cell types, we employed the CellChat R package (v2.1.1) [119,120] to infer ligand-receptor pairs between cell types. In brief, we subset only signaling genes from the expression matrix, identified over-expressed ligands and receptors, and determined over-expressed ligand-receptor interactions. Biologically significant cell-cell communications were inferred using the statistically robust *triMean* method. We then computed the communication probability at the signaling pathway level by summarizing the communication probabilities of all ligand-receptor interactions associated with each pathway.

Statistical analysis

All data are represented as mean ± SEM. When only two independent groups were compared, significance was determined by using a two-tailed unpaired t-test with Welch's correction. A p-value of < 0.05 was considered significant. All the analyses were done in GraphPad Prism v.9.

Figure legends

Fig 1. Generation and characterization of hMAN chimeric mice

(A) A schematic diagram showing that hiPSC and hESC-derived PMPs and pNPCs are engrafted into the brains of P0 *Rag2*$^{-/-}$ *IL2rγ*$^{-/-}$ *hCSF1*^{KI} mice.

(B) Representative image from sagittal brain sections showing the distribution of hN^{+} xenografted cells at 7 months post-transplantation. Scale bar: 1 mm and 50 μm in the original or enlarged images, respectively. Arrowheads in B1 and B2 indicate cells that have migrated and integrated with mouse cells at the periphery of the cluster of engrafted human cells.

(C and D) Representative images (C) and quantification (D) of NeuN^{+}, OLIG2^{+}, GFAP^{+}, and IBA-expressing cells (n = 4 mice). Scale bars: 20 μm and 5 μm in the original or enlarged images, respectively.

(E and F) Representative images and quantification (F) of hMAP2^{+}, GLS^{+}, and GABA-expressing cells (n = 3 mice). Scale bars: 20 μm and 10 μm in the original or enlarged images, respectively.

(G) Representative images of hMAP2^{+} and hTMEM119-expressing cells. Scale bars:100 μm.

(H) Representative raw fluorescent super-resolution and 3D surface rendered images showing colocalization of hTMEM119^{+} and hN^{+} staining. Scale bars: 20 μm and 1 μm in the original and enlarged images, respectively.

(I) Representative raw fluorescent super-resolution and 3D surface rendered images showing colocalization of hTMEM119^{+} and hSynaptophysin^{+} staining. Scale bars: 5 μm and 1 μm in the original and enlarged images, respectively

(J) Representative raw fluorescent super-resolution and 3D surface rendered images showing colocalization of hCD45^{+} and TBR2^{+} staining. Scale bars: 5 μm and 1 μm in the original and enlarged images, respectively.

(K) Representative images of hCD44^{+} and GFAP-expressing cells with extended long, unbranched processes. Scale bars: 50 μm.

(L) Representative images of hCD44^{+} and S100B-expressing cells. Scale bars: 20 μm.

(M) Representative images of hCD44^{+} and GFAP-expressing cells. Scale bars: 20 μm.

Fig 2. Generation and characterization of hMON chimeric mice

(A) A schematic diagram showing that hiPSC and hESC-derived PMPs and pNPCs are engrafted into the brains of P0 *shi/shi x Rag2*$^{-/-}$ mice.

(B) Representative image from sagittal brain sections showing the distribution of hN^{+} xenografted cells at 4 months post-transplantation. Scale bar: 1 mm and 50 μm in the original or enlarged images, respectively. Arrowheads in B1 and B2 indicate cells that have migrated and integrated with mouse cells at the periphery of the cluster of engrafted human cells.

(C and D) Representative images (C) and quantification (D) of NeuN^{+}, OLIG2^{+}, GFAP^{+}, and IBA-expressing cells (n = 3 mice). Scale bars: 20 μm and 5 μm in the original or enlarged images, respectively.

(E) Representative images of NG2^{+} and hN-expressing cells. Scale bars: 100 μm.

(F) Representative images of MBP^{+} and hN^{+} cells. Scale bars: 20 μm.

(G) Representative raw fluorescent super-resolution and 3D surface rendered images showing colocalization of hMAP2^{+} and MBP^{+} staining. Scale bars: 5 μm and 1 μm in the original and enlarged images, respectively.

(H and I) Representative images (H) and quantification (I) of DAPI and hNG2-expressing cells in *shi/shi x Rag2*$^{-/-}$ *and Rag2*$^{-/-}$ *IL2rγ*$^{-/-}$ *hCSF1*^{KI} mice (n = 4 mice/group). Student's t test, *, p value < 0.05. Scale bars: 100 μm.

Fig 3. Generation and characterization of co-transplantation of PMPs and ventralized NPCs into mouse brains

(A) A schematic procedure for deriving microglia-containing brain organoids by co-culture of ventralized NPCs and PMPs under 3D conditions. Scale bars: 400 μm.
(B and C) Representative images (B) and quantification (C) of PU.1$^+$/CD45$^+$ cells in day 9 brain organoids (n = 3 from three independent experiments). Scale bars, 20 μm.
(D) Representative images of CD45$^+$ cells in one-month organoids. Scale bar, 20 μm.
(E) Representative raw fluorescent super-resolution and 3D surface rendered images showing colocalization of SOX2$^+$ and hTMEM119$^+$ cells in one-month organoids. Scale bars, 20 μm, 5 μm and 5 μm in the original and enlarged images, respectively.
(F) Representative images of TUJ-1$^+$ and GABA$^+$ cells in one-month organoids. Scale bars: 20 μm.
(G) Representative images of S100B$^+$ cells in one-month organoids. Scale bars: 20 μm.
(H) Quantification of SOX2$^+$, TUJ-1$^+$, GABA$^+$, S100B$^+$, and hTMEM119$^+$ cells in one-month organoids (n = 3 from three independent experiments).
(I) qPCR analysis of CSF1, IL-34, and IBA-1 mRNA in one-month organoids (n = 4 from four independent experiments). Student's t test, *, p value < 0.05.
(J) A schematic diagram showing that hiPSC and hESC-derived PMP and v-NPCs are engrafted into the brains of P0 *Rag2*$^{-/-}$ mice.
(K and L) Representative images (K) and quantification (L) of NeuN$^+$, OLIG2$^+$, GFAP$^+$, and IBA-expressing cells in the brains of *Rag2*$^{-/-}$ mouse (n = 3 mice). Scale bars: 20 μm.

Fig 4. scRNA-seq analyses of hMAN chimeric brain

(A) UMAP plot of scRNA-seq data (n = 23,994 human cells) from 3-month-old *Rag2*$^{-/-}$ IL2rγ$^{-/-}$ *hCSF1*^{KI} hMAN chimeric brains.
(B) Dot plot showing expression of key marker genes of each annotated human cell type (NPC, neural progenitor cell; GPC, glia progenitor cell; Astro, astrocyte; VLMC, vascular leptomeningeal cell).
(C) Dot plot showing expression of marker genes of macroglia human cell types (OPC, oligodendrocyte precursor cell; Oligo., oligodendrocyte).
(D) Heatmap showing the significant overlap of marker genes between human cortical macroglia (Veleshev et al.) and this study. Jaccard score represents the percentage of pairwise overlapping genes. Fisher's exact test is used to evaluate the significance of overlapping (The significant levels are represented by stars (N.S., not significant).
(E) Representative images of hN$^+$ and ETV4$^+$ cells from 2-month-old *Rag2*$^{-/-}$ IL2rγ$^{-/-}$ *hCSF1*^{KI} hMAN chimeric brains. Scale bar, 20 μm.
(F) UMAP plot of astrocyte subclusters (n = 11,100 cells).
(G) UMAP plot of astrocyte subclusters, each cell is colored by its pseudotime trajectory assignment.
(H) Dot plot showing expression of marker genes of each astrocyte subcluster.
(I) Heatmap showing the significant overlap of marker genes between astrocyte subtypes of human hippocampus astrocytes (Su et al.) and this study. Jaccard score represents the percentage of pairwise overlapping genes. Fisher's exact test is used to evaluate the significance of overlapping (The significant levels are represented by stars (N.S., not significant; *, p value < 0.05; **, p value < 0.01; ***, p value < 0.001; ****, p value < 0.0001).
(J) Chord diagram showing inferred cell-cell interaction weights/strength between cell types. The thickness of the line represents the weight of ligand-receptor pairs scaled by cell type population.
(K) Bubble plot showing the ligand-receptor interactions between neurons and glia.
(L) Heatmap showing the interaction weight between cell types of the APP signaling pathway.
(M) Chord diagram showing the interaction weight between cell types of the NRXN signaling pathway.
(N) Bubble plot showing the ligand-receptor interactions between glial cell types.
(O) Heatmap showing the centrality scores/importance of cell groups as senders, receivers, mediators and influencers in the PTN signaling pathway and MK signaling pathway.
(P) Chord diagram showing the significant interaction pairs involved in the NOTCH signaling pathways.

Fig S1. Related to Fig 1.
(A and B) Representative images (A) and quantification (B) of $CD43^+$ and $CD235^+$ cells in PMPs, and $SOX2^+$ and $PAX6^+$ cells in pNPCs (n = 3 from three independent experiments). Scale bars, 20 μm.
(C) Heatmap showing expression of signature genes of pNPCs and PMPs from RNA-seq data (n = 3 for pNPC, n = 3 for PMP,).
(D) Bar plot showing the expression level of pluripotency markers (NANOG and POU5F1/OCT4) expression of pNPCs.
(E) Representative images from sagittal brain sections showing the distribution of hN^+ xenografted cells at 7 months post-transplantation. Scale bar: 1 mm.
(F) Representative images of $NeuN^+$, $OLIG2^+$, $GFAP^+$, and IBA^+-expressing cells. Scale bars: 20 μm.
(G) Quantification of $NeuN^+$, $OLIG2^+$, $GFAP^+$, and IBA^+-expressing cells in hN^+ cells (n = 3 mice).
(H) Quantification of $S100B^+$, $S100B^-$, $GFAP^+$, and $GFAP^-$ cells in $hCD44^+$ cells (n = 3 mice).
(I) Representative images of $OCT4^+$ expressing cells in hiPSCs and 7-month-old *Rag2*$^{-/-}$ *IL2rγ*$^{-/-}$ *hCSF1*^{KI} mice. Scale bars: 20 μm.
(J and K) Representative images (J) and quantification (K) of $Ki67^+$ in 7-month-old *Rag2*$^{-/-}$ *IL2rγ*$^{-/-}$ *hCSF1*^{KI} mice (n = 3 mice). Scale bars: 20 μm.

Fig S2. Related to Fig 2.
(A) Representative images from sagittal brain sections showing the distribution of hN^+ xenografted cells at 4 months post transplantation. Scale bar: 1 mm.
(B) Representative images of $OCT4^+$ expressing cells in hiPSCs and 4-month-old *shi/shi x Rag2*$^{-/-}$ mice. Scale bars: 20 μm.
(C and D) Representative images (C) and quantification (D) of $Ki67^+$ cells in 4-month-old *shi/shi x Rag2*$^{-/-}$ mouse brains (n = 3 from three independent experiments). Scale bars, 20 μm.
(E) Representative images of $NeuN^+$, GFP^+, $OLIG2^+$, $IBA1^+$, and hN^+ cells in the brains of 3-month-old *Rag1*$^{-/-}$ mice. Scale bars, 20 μm.
(F) Representative raw fluorescent super-resolution and 3D surface rendered images showing colocalization of hCD45 and DAPI staining. Scale bars: 5 μm.
(G) Representative images of $hMAP2^+$ cells in the brains of 3-month-old *shi/shi x Rag2*$^{-/-}$ mice. Scale bars, 200 μm.
(H) Representative images of $hMAP2^+$, and $GABA^+$-expressing cells in the brains of 3-month-old *shi/shi x Rag2*$^{-/-}$ mice. Scale bars, 20 μm.

Fig S3. Related to Fig 3.
(A) Representative images and quantification of $NKX2.1^+$, $PAX6^+$, and $OLIG2^+$-expressing cells after 1 week of patterning (n = 3 from three independent experiments). Scale bars: 20 μm.
(B) Representative images of $hMAP2^+$ and $GABA^+$ cells in the brains of *Rag2*$^{-/-}$ mouse. Arrows indicate $hMAP2^+GABA^+$ inhibitory neurons; Arrowheads indicate $hMAP2^+GABA^-$ excitatory neurons. Scale bars: 20 μm.

Fig S4. Related to Fig 4.
(A) Violin plots showing the quality control matrices after filtration from two libraries: gene numbers per cell (*nFeature_RNA*), UMIs per cell (*nCount_RNA*), and percentage of mitochondria genes per cell (*percent. mt*).
(B) Dot plot showing expression of key marker genes of each annotated human cell type.
(C) UMAP plot of 19 clusters and annotations identified from 3-month-old *Rag2*$^{-/-}$ *IL2rγ*$^{-/-}$ *hCSF1*^{KI} hMAN chimeric brains.
(D) Bar plot showing proportion of cell cycle phases in each cell type.
(E) Dot plot showing expression of proliferation and pluripotency markers in cycling cell types.
(F) Heatmap showing the CNV profiles inferred from gene expression data.

(G) Ridgeline plot of predicted ages of hMAN cells and cortical organoid transplants.
(H) Representative images of hNG2^{+}/ETV4^{+} and hNG2^{-}/ETV4^{+} cells from 2-month-old *Rag2*$^{-/-}$ *IL2rγ*$^{-/-}$ *hCSF1*^{KI} hMAN chimeric brains. Scale bar, 5 μm.
(I) Dot plot showing expression of *THY1*, *EGFR*, and *PDGFRA* genes.
(J) Chord diagram showing the significant interaction pairs involved in the neuron-glia interactions.
(K) Chord diagram showing the significant interaction pairs involved in the glia-glia interactions.

Supplementary Table 1. A list of antibodies used.

Antibodies	SOURCE	IDENTIFIER
Mouse anti-human nuclei	Millipore	RRID: AB_827439
Rabbit anti-NeuN (Neuronal nuclei)	Millipore	RRID: AB_2298772
Rabbit anti-OLIG2 (Oligodendrocyte transcription factor 2)	Phosphosolutions	RRID: AB_2492193
Rabbit anti-GFAP (Glial fibrillary acidic protein)	Millipore	RRID: AB_2109645
Rabbit anti-IBA1 (Ionized calcium-binding adapter molecule 1)	Wako	RRID: AB_ 839504
Mouse anti-MAP2 (Microtubule associated protein 2)	Santa Cruz Biotechnologies	RRID: AB_1126219
Rabbit anti-GLS (Glutaminase)	Abcam	RRID: AB_2721038
Rabbit anti-GABA (Gamma-aminobutyric acid)	Millipore	RRID: AB_477652
Rabbit anti-TMEM119 (Transmembrane protein 119)	Invitrogen	RRID: AB_2648507
Mouse anti-Synaptophysin	Invitrogen	RRID: AB_10670280
Mouse anti-CD44 (HCAM, Homing cell adhesion molecule)	Abcam	RRID: AB_305297
Rabbit anti-S100B (S100 calcium-binding protein B)	Sigma	RRID: AB_477499
Mouse anti-CD45 (PTPRC, protein tyrosine phosphatase receptor type C)	Invitrogen	RRID: AB_11063696
Rabbit anti-TBR2 (T-box brain protein 2)	Abcam	RRID: AB_778267
Mouse anti-CD43 (Cluster of differentiation 43)	Invitrogen	RRID: AB_763493
Rabbit anti-CD235 (Cluster of differentiation 235)	Invitrogen	RRID: AB_90757
Mouse anti-SOX2 (SRY-box transcription factor 2)	Santa Cruz Biotechnologies	RRID: AB_10842165
Rabbit anti-PAX6 (Paired box 6)	GeneTex	RRID: AB_1951119
Rabbit anti-NG2 (Neuron-glial antigen 2)	Millipore	RRID: AB_91789
Rat anti-MBP (Myelin basic	Millipore	RRID: AB_94975

protein)		
Rabbit anti-PU.1 (SPI1, Spi-1 proto-oncogene)	Invitrogen	RRID: AB_11150963
Mouse anti-bIIItubulin	Millipore	RRID: AB_2210524
Rabbit anti-NKX2.1(TTF1) (Thyroid transcription factor 1)	Abcam	RRID: AB_1310784
Mouse-NKX2.1(TTF1) (Thyroid transcription factor 1)	Sigma	RRID: AB_571072
Rabbit anti-ETV4 (ETS translocation variant 4)	Abcam	RRID: AB_3095819
Mouse anti-NG2 (Neuron-glial antigen 2)	Millipore	RRID: AB_94509
Rabbit anti-PDGF (Platelet-derived growth factor，alpha)	Cell Signaling Technology	RRID: AB_10692773
Rabbit anti-Ki-67 (Marker of proliferation Kiel 67)	Thermo Fisher Scientific	RRID:AB_10979488
Rabbit anti-OCT4 (Octamer-binding transcription factor 4)	Cell Signaling Technology	RRID:AB_2167691
Goat Anti-mouse 488	Thermo Fisher Scientific	RRID: AB_2534088
Goat Anti-mouse 594	Thermo Fisher Scientific	RRID: AB_2534079
Goat Anti-mouse 647	Thermo Fisher Scientific	RRID: AB_2535804
Goat Anti-rabbit 488	Thermo Fisher Scientific	RRID: AB_143165
Goat Anti-rabbit 594	Thermo Fisher Scientific	RRID: AB_2534073
Goat Anti-rabbit 647	Thermo Fisher Scientific	RRID: AB_2535813
Goat Anti-rat 594	Thermo Fisher Scientific	RRID: AB_10561522

Supplementary Table 2. Taqman Primers.

Gene	**Full name**	**Gene expression assay catalog number**
IL-34	Interleukin-34	Hs01050926_m1
AIF1 (IBA1)	Allograft Inflammatory Factor 1	Hs00610419_g1
CSF1	Colony stimulating factor 1	Hs00174164_m1
GAPDH (human specific)	Glyceraldehyde-3-Phosphate Dehydrogenase	Hs04420697_g1

References

1. Gao, Y., Hong, Y., Huang, L., Zheng, S., Zhang, H., Wang, S., Yao, Y., Zhao, Y., Zhu, L., Xu, Q., et al. (2023). beta2-microglobulin functions as an endogenous NMDAR antagonist to impair synaptic function. Cell *186*, 1026-1038 e1020. 10.1016/j.cell.2023.01.021.
2. Yin, Z., Rosenzweig, N., Kleemann, K.L., Zhang, X., Brandao, W., Margeta, M.A., Schroeder, C., Sivanathan, K.N., Silveira, S., Gauthier, C., et al. (2023). APOE4 impairs the microglial response in Alzheimer's disease by inducing TGFbeta-mediated checkpoints. Nat Immunol *24*, 1839-1853. 10.1038/s41590-023-01627-6.
3. Chen, X., Firulyova, M., Manis, M., Herz, J., Smirnov, I., Aladyeva, E., Wang, C., Bao, X., Finn, M.B., Hu, H., et al. (2023). Microglia-mediated T cell infiltration drives neurodegeneration in tauopathy. Nature *615*, 668-677. 10.1038/s41586-023-05788-0.
4. Avior, Y., Sagi, I., and Benvenisty, N. (2016). Pluripotent stem cells in disease modelling and drug discovery. Nat Rev Mol Cell Biol *17*, 170-182. 10.1038/nrm.2015.27.
5. Qian, X., Nguyen, H.N., Song, M.M., Hadiono, C., Ogden, S.C., Hammack, C., Yao, B., Hamersky, G.R., Jacob, F., Zhong, C., et al. (2016). Brain-Region-Specific Organoids Using Mini-bioreactors for Modeling ZIKV Exposure. Cell *165*, 1238-1254. 10.1016/j.cell.2016.04.032.
6. Kelley, K.W., and Pasca, S.P. (2022). Human brain organogenesis: Toward a cellular understanding of development and disease. Cell *185*, 42-61. 10.1016/j.cell.2021.10.003.
7. Qian, X., Song, H., and Ming, G.L. (2019). Brain organoids: advances, applications and challenges. Development *146*. 10.1242/dev.166074.
8. Xu, R., Boreland, A.J., Li, X., Erickson, C., Jin, M., Atkins, C., Pang, Z.P., Daniels, B.P., and Jiang, P. (2021). Developing human pluripotent stem cell-based cerebral organoids with a controllable microglia ratio for modeling brain development and pathology. Stem cell reports *16*, 1923-1937. 10.1016/j.stemcr.2021.06.011.
9. Patterson, M., Chan, D.N., Ha, I., Case, D., Cui, Y., Van Handel, B., Mikkola, H.K., and Lowry, W.E. (2012). Defining the nature of human pluripotent stem cell progeny. Cell Res *22*, 178-193. 10.1038/cr.2011.133.
10. Di Lullo, E., and Kriegstein, A.R. (2017). The use of brain organoids to investigate neural development and disease. Nat Rev Neurosci *18*, 573-584. 10.1038/nrn.2017.107.
11. Jiang, P., and Alam, M.M. (2022). Rise of the human-mouse chimeric brain models. Cell Regen *11*, 32. 10.1186/s13619-022-00135-6.
12. Jiang, P., Turkalj, L., and Xu, R. (2020). High-Fidelity Modeling of Human Microglia with Pluripotent Stem Cells. Cell Stem Cell *26*, 629-631. 10.1016/j.stem.2020.04.004.
13. Xu, R., Li, X., Boreland, A.J., Posyton, A., Kwan, K., Hart, R.P., and Jiang, P. (2020). Human iPSC-derived mature microglia retain their identity and functionally integrate in the chimeric mouse brain. Nat Commun *11*, 1577. 10.1038/s41467-020-15411-9.
14. Jin, M., Xu, R., Wang, L., Alam, M.M., Ma, Z., Zhu, S., Martini, A.C., Jadali, A., Bernabucci, M., Xie, P., et al. (2022). Type-I-interferon signaling drives microglial dysfunction and senescence in human iPSC models of Down syndrome and Alzheimer's disease. Cell Stem Cell *29*, 1135-1153 e1138. 10.1016/j.stem.2022.06.007.
15. Hasselmann, J., Coburn, M.A., England, W., Figueroa Velez, D.X., Kiani Shabestari, S., Tu, C.H., McQuade, A., Kolahdouzan, M., Echeverria, K., Claes, C., et al. (2019). Development of a Chimeric Model to Study and Manipulate Human Microglia In Vivo. Neuron *103*, 1016-1033 e1010. 10.1016/j.neuron.2019.07.002.
16. Mancuso, R., Fattorelli, N., Martinez-Muriana, A., Davis, E., Wolfs, L., Van Den Daele, J., Geric, I., Premereur, J., Polanco, P., Bijnens, B., et al. (2024). Xenografted human microglia display diverse transcriptomic states in response to Alzheimer's disease-related amyloid-beta pathology. Nat Neurosci. 10.1038/s41593-024-01600-y.
17. Windrem, M.S., Osipovitch, M., Liu, Z., Bates, J., Chandler-Militello, D., Zou, L., Munir, J., Schanz, S., McCoy, K., Miller, R.H., et al. (2017). Human iPSC Glial Mouse Chimeras Reveal

Glial Contributions to Schizophrenia. Cell Stem Cell *21*, 195-208 e196. 10.1016/j.stem.2017.06.012.

18. Linaro, D., Vermaercke, B., Iwata, R., Ramaswamy, A., Libe-Philippot, B., Boubakar, L., Davis, B.A., Wierda, K., Davie, K., Poovathingal, S., et al. (2019). Xenotransplanted Human Cortical Neurons Reveal Species-Specific Development and Functional Integration into Mouse Visual Circuits. Neuron *104*, 972-986 e976. 10.1016/j.neuron.2019.10.002.
19. Balusu, S., Horre, K., Thrupp, N., Craessaerts, K., Snellinx, A., Serneels, L., T'Syen, D., Chrysidou, I., Arranz, A.M., Sierksma, A., et al. (2023). MEG3 activates necroptosis in human neuron xenografts modeling Alzheimer's disease. Science *381*, 1176-1182. 10.1126/science.abp9556.
20. Real, R., Peter, M., Trabalza, A., Khan, S., Smith, M.A., Dopp, J., Barnes, S.J., Momoh, A., Strano, A., Volpi, E., et al. (2018). In vivo modeling of human neuron dynamics and Down syndrome. Science *362*. 10.1126/science.aau1810.
21. Wang, M., Gage, F.H., and Schafer, S.T. (2023). Transplantation Strategies to Enhance Maturity and Cellular Complexity in Brain Organoids. Biol Psychiatry *93*, 616-621. 10.1016/j.biopsych.2023.01.004.
22. Mansour, A.A., Goncalves, J.T., Bloyd, C.W., Li, H., Fernandes, S., Quang, D., Johnston, S., Parylak, S.L., Jin, X., and Gage, F.H. (2018). An in vivo model of functional and vascularized human brain organoids. Nat Biotechnol *36*, 432-441. 10.1038/nbt.4127.
23. Revah, O., Gore, F., Kelley, K.W., Andersen, J., Sakai, N., Chen, X., Li, M.Y., Birey, F., Yang, X., Saw, N.L., et al. (2022). Maturation and circuit integration of transplanted human cortical organoids. Nature *610*, 319-326. 10.1038/s41586-022-05277-w.
24. Schafer, S.T., Mansour, A.A., Schlachetzki, J.C.M., Pena, M., Ghassemzadeh, S., Mitchell, L., Mar, A., Quang, D., Stumpf, S., Ortiz, I.S., et al. (2023). An in vivo neuroimmune organoid model to study human microglia phenotypes. Cell *186*, 2111-2126.e2120. 10.1016/j.cell.2023.04.022.
25. Wang, M., Zhang, L., Novak, S.W., Yu, J., Gallina, I.S., Xu, L.L., Lim, C.K., Fernandes, S., Shokhirev, M.N., Williams, A.E., et al. (2024). Morphological diversification and functional maturation of human astrocytes in glia-enriched cortical organoid transplanted in mouse brain. Nat Biotechnol. 10.1038/s41587-024-02157-8.
26. Allen, N.J., and Lyons, D.A. (2018). Glia as architects of central nervous system formation and function. Science *362*, 181-185. 10.1126/science.aat0473.
27. Prinz, M., Jung, S., and Priller, J. (2019). Microglia Biology: One Century of Evolving Concepts. Cell *179*, 292-311. 10.1016/j.cell.2019.08.053.
28. Verkhratsky, A., and Nedergaard, M. (2018). Physiology of Astroglia. Physiol Rev *98*, 239-389. 10.1152/physrev.00042.2016.
29. Simons, M., and Nave, K.A. (2015). Oligodendrocytes: Myelination and Axonal Support. Cold Spring Harb Perspect Biol *8*, a020479. 10.1101/cshperspect.a020479.
30. Gosselin, D., Skola, D., Coufal, N.G., Holtman, I.R., Schlachetzki, J.C.M., Sajti, E., Jaeger, B.N., O'Connor, C., Fitzpatrick, C., Pasillas, M.P., et al. (2017). An environment-dependent transcriptional network specifies human microglia identity. Science *356*. 10.1126/science.aal3222.
31. Galatro, T.F., Holtman, I.R., Lerario, A.M., Vainchtein, I.D., Brouwer, N., Sola, P.R., Veras, M.M., Pereira, T.F., Leite, R.E.P., Moller, T., et al. (2017). Transcriptomic analysis of purified human cortical microglia reveals age-associated changes. Nat Neurosci *20*, 1162-1171. 10.1038/nn.4597.
32. Oberheim, N.A., Takano, T., Han, X., He, W., Lin, J.H., Wang, F., Xu, Q., Wyatt, J.D., Pilcher, W., Ojemann, J.G., et al. (2009). Uniquely hominid features of adult human astrocytes. J Neurosci *29*, 3276-3287. 10.1523/JNEUROSCI.4707-08.2009.
33. Oberheim, N.A., Wang, X., Goldman, S., and Nedergaard, M. (2006). Astrocytic complexity distinguishes the human brain. Trends Neurosci *29*, 547-553. 10.1016/j.tins.2006.08.004.

34. Han, X., Chen, M., Wang, F., Windrem, M., Wang, S., Shanz, S., Xu, Q., Oberheim, N.A., Bekar, L., Betstadt, S., et al. (2013). Forebrain engraftment by human glial progenitor cells enhances synaptic plasticity and learning in adult mice. Cell Stem Cell *12*, 342-353. 10.1016/j.stem.2012.12.015.
35. Hawrylycz, M.J., Lein, E.S., Guillozet-Bongaarts, A.L., Shen, E.H., Ng, L., Miller, J.A., van de Lagemaat, L.N., Smith, K.A., Ebbert, A., Riley, Z.L., et al. (2012). An anatomically comprehensive atlas of the adult human brain transcriptome. Nature *489*, 391-399. 10.1038/nature11405.
36. Xu, R., Brawner, A.T., Li, S., Liu, J.J., Kim, H., Xue, H., Pang, Z.P., Kim, W.Y., Hart, R.P., Liu, Y., and Jiang, P. (2019). OLIG2 Drives Abnormal Neurodevelopmental Phenotypes in Human iPSC-Based Organoid and Chimeric Mouse Models of Down Syndrome. Cell Stem Cell *24*, 908-926 e908. 10.1016/j.stem.2019.04.014.
37. Xu, R., Boreland, A.J., Li, X., Erickson, C., Jin, M., Atkins, C., Pang, Z.P., Daniels, B.P., and Jiang, P. (2021). Developing human pluripotent stem cell-based cerebral organoids with a controllable microglia ratio for modeling brain development and pathology. Stem Cell Reports. 10.1016/j.stemcr.2021.06.011.
38. Cardona, C., Sanchez-Mejias, E., Davila, J.C., Martin-Rufian, M., Campos-Sandoval, J.A., Vitorica, J., Alonso, F.J., Mates, J.M., Segura, J.A., Norenberg, M.D., et al. (2015). Expression of Gls and Gls2 glutaminase isoforms in astrocytes. Glia *63*, 365-382. 10.1002/glia.22758.
39. Paolicelli, R.C., Bolasco, G., Pagani, F., Maggi, L., Scianni, M., Panzanelli, P., Giustetto, M., Ferreira, T.A., Guiducci, E., Dumas, L., et al. (2011). Synaptic pruning by microglia is necessary for normal brain development. Science *333*, 1456-1458. 10.1126/science.1202529.
40. Liu, Y., Han, S.S., Wu, Y., Tuohy, T.M., Xue, H., Cai, J., Back, S.A., Sherman, L.S., Fischer, I., and Rao, M.S. (2004). CD44 expression identifies astrocyte-restricted precursor cells. Dev Biol *276*, 31-46. 10.1016/j.ydbio.2004.08.018.
41. Dzwonek, J., and Wilczynski, G.M. (2015). CD44: molecular interactions, signaling and functions in the nervous system. Front Cell Neurosci *9*, 175. 10.3389/fncel.2015.00175.
42. Pan, G.J., Chang, Z.Y., Scholer, H.R., and Pei, D. (2002). Stem cell pluripotency and transcription factor Oct4. Cell Res *12*, 321-329. 10.1038/sj.cr.7290134.
43. Wang, Y.J., and Herlyn, M. (2015). The emerging roles of Oct4 in tumor-initiating cells. Am J Physiol Cell Physiol *309*, C709-718. 10.1152/ajpcell.00212.2015.
44. Windrem, M.S., Schanz, S.J., Morrow, C., Munir, J., Chandler-Militello, D., Wang, S., and Goldman, S.A. (2014). A competitive advantage by neonatally engrafted human glial progenitors yields mice whose brains are chimeric for human glia. J Neurosci *34*, 16153-16161. 10.1523/JNEUROSCI.1510-14.2014.
45. Chen, C., Kim, W.Y., and Jiang, P. (2016). Humanized neuronal chimeric mouse brain generated by neonatally engrafted human iPSC-derived primitive neural progenitor cells. JCI Insight *1*, e88632. 10.1172/jci.insight.88632.
46. Chen, C., Jiang, P., Xue, H., Peterson, S.E., Tran, H.T., McCann, A.E., Parast, M.M., Li, S., Pleasure, D.E., Laurent, L.C., et al. (2014). Role of astroglia in Down's syndrome revealed by patient-derived human-induced pluripotent stem cells. Nat Commun *5*, 4430. 10.1038/ncomms5430.
47. Roach, A., Boylan, K., Horvath, S., Prusiner, S.B., and Hood, L.E. (1983). Characterization of cloned cDNA representing rat myelin basic protein: absence of expression in brain of shiverer mutant mice. Cell *34*, 799-806. 10.1016/0092-8674(83)90536-6.
48. Rosenbluth, J. (1980). Central myelin in the mouse mutant shiverer. J Comp Neurol *194*, 639-648. 10.1002/cne.901940310.
49. Liu, S., Qu, Y., Stewart, T.J., Howard, M.J., Chakrabortty, S., Holekamp, T.F., and McDonald, J.W. (2000). Embryonic stem cells differentiate into oligodendrocytes and myelinate in culture and after spinal cord transplantation. Proc Natl Acad Sci U S A *97*, 6126-6131. 10.1073/pnas.97.11.6126.

50. Jiang, P., Chen, C., Liu, X.B., Selvaraj, V., Liu, W., Feldman, D.H., Liu, Y., Pleasure, D.E., Li, R.A., and Deng, W. (2013). Generation and characterization of spiking and nonspiking oligodendroglial progenitor cells from embryonic stem cells. Stem cells *31*, 2620-2631. 10.1002/stem.1515.
51. Easley-Neal, C., Foreman, O., Sharma, N., Zarrin, A.A., and Weimer, R.M. (2019). CSF1R Ligands IL-34 and CSF1 Are Differentially Required for Microglia Development and Maintenance in White and Gray Matter Brain Regions. Front Immunol *10*, 2199. 10.3389/fimmu.2019.02199.
52. Han, R.T., Kim, R.D., Molofsky, A.V., and Liddelow, S.A. (2021). Astrocyte-immune cell interactions in physiology and pathology. Immunity *54*, 211-224. 10.1016/j.immuni.2021.01.013.
53. Cahoy, J.D., Emery, B., Kaushal, A., Foo, L.C., Zamanian, J.L., Christopherson, K.S., Xing, Y., Lubischer, J.L., Krieg, P.A., Krupenko, S.A., et al. (2008). A transcriptome database for astrocytes, neurons, and oligodendrocytes: a new resource for understanding brain development and function. J Neurosci *28*, 264-278. 10.1523/JNEUROSCI.4178-07.2008.
54. Kim, H., Xu, R., Padmashri, R., Dunaevsky, A., Liu, Y., Dreyfus, C.F., and Jiang, P. (2019). Pluripotent Stem Cell-Derived Cerebral Organoids Reveal Human Oligodendrogenesis with Dorsal and Ventral Origins. Stem cell reports *12*, 890-905. 10.1016/j.stemcr.2019.04.011.
55. McKercher, S.R., Torbett, B.E., Anderson, K.L., Henkel, G.W., Vestal, D.J., Baribault, H., Klemsz, M., Feeney, A.J., Wu, G.E., Paige, C.J., and Maki, R.A. (1996). Targeted disruption of the PU.1 gene results in multiple hematopoietic abnormalities. EMBO J *15*, 5647-5658.
56. iPS-cell-derived microglia promote brain organoid maturation via cholesterol transfer. (2023). Nature. 10.1038/s41586-023-06713-1.
57. Park, D.S., Kozaki, T., Tiwari, S.K., Moreira, M., Khalilnezhad, A., Torta, F., Olivie, N., Thiam, C.H., Liani, O., Silvin, A., et al. (2023). iPS-cell-derived microglia promote brain organoid maturation via cholesterol transfer. Nature *623*, 397-405. 10.1038/s41586-023-06713-1.
58. Herring, C.A., Simmons, R.K., Freytag, S., Poppe, D., Moffet, J.J.D., Pflueger, J., Buckberry, S., Vargas-Landin, D.B., Clement, O., Echeverria, E.G., et al. (2022). Human prefrontal cortex gene regulatory dynamics from gestation to adulthood at single-cell resolution. Cell *185*, 4428-4447 e4428. 10.1016/j.cell.2022.09.039.
59. Velmeshev, D., Perez, Y., Yan, Z., Valencia, J.E., Castaneda-Castellanos, D.R., Wang, L., Schirmer, L., Mayer, S., Wick, B., Wang, S., et al. (2023). Single-cell analysis of prenatal and postnatal human cortical development. Science *382*, eadf0834. 10.1126/science.adf0834.
60. Liu, D.D., He, J.Q., Sinha, R., Eastman, A.E., Toland, A.M., Morri, M., Neff, N.F., Vogel, H., Uchida, N., and Weissman, I.L. (2023). Purification and characterization of human neural stem and progenitor cells. Cell *186*, 1179-1194 e1115. 10.1016/j.cell.2023.02.017.
61. Su, Y., Zhou, Y., Bennett, M.L., Li, S., Carceles-Cordon, M., Lu, L., Huh, S., Jimenez-Cyrus, D., Kennedy, B.C., Kessler, S.K., et al. (2022). A single-cell transcriptome atlas of glial diversity in the human hippocampus across the postnatal lifespan. Cell Stem Cell *29*, 1594-1610 e1598. 10.1016/j.stem.2022.09.010.
62. Manocha, G.D., Floden, A.M., Rausch, K., Kulas, J.A., McGregor, B.A., Rojanathammanee, L., Puig, K.R., Puig, K.L., Karki, S., Nichols, M.R., et al. (2016). APP Regulates Microglial Phenotype in a Mouse Model of Alzheimer's Disease. J Neurosci *36*, 8471-8486. 10.1523/JNEUROSCI.4654-15.2016.
63. Kim, H., Kim, D., Kim, J., Lee, H.Y., Park, D., Kang, H., Matsuda, K., Sterky, F.H., Yuzaki, M., Kim, J.Y., et al. (2020). Calsyntenin-3 interacts with both alpha- and beta-neurexins in the regulation of excitatory synaptic innervation in specific Schaffer collateral pathways. J Biol Chem *295*, 9244-9262. 10.1074/jbc.RA120.013077.
64. Lipina, T.V., Prasad, T., Yokomaku, D., Luo, L., Connor, S.A., Kawabe, H., Wang, Y.T., Brose, N., Roder, J.C., and Craig, A.M. (2016). Cognitive Deficits in Calsyntenin-2-deficient Mice Associated with Reduced GABAergic Transmission. Neuropsychopharmacology *41*, 802-810. 10.1038/npp.2015.206.

65. Ster, J., Steuble, M., Orlando, C., Diep, T.M., Akhmedov, A., Raineteau, O., Pernet, V., Sonderegger, P., and Gerber, U. (2014). Calsyntenin-1 regulates targeting of dendritic NMDA receptors and dendritic spine maturation in CA1 hippocampal pyramidal cells during postnatal development. J Neurosci *34*, 8716-8727. 10.1523/JNEUROSCI.0144-14.2014.
66. Sudhof, T.C. (2008). Neuroligins and neurexins link synaptic function to cognitive disease. Nature *455*, 903-911. 10.1038/nature07456.
67. Lin, E.Y., Xi, W., Aggarwal, N., and Shinohara, M.L. (2023). Osteopontin (OPN)/SPP1: from its biochemistry to biological functions in the innate immune system and the central nervous system (CNS). Int Immunol *35*, 171-180. 10.1093/intimm/dxac060.
68. Sorrelle, N., Dominguez, A.T.A., and Brekken, R.A. (2017). From top to bottom: midkine and pleiotrophin as emerging players in immune regulation. J Leukoc Biol *102*, 277-286. 10.1189/jlb.3MR1116-475R.
69. Xu, C., Zhu, S., Wu, M., Han, W., and Yu, Y. (2014). Functional receptors and intracellular signal pathways of midkine (MK) and pleiotrophin (PTN). Biol Pharm Bull *37*, 511-520. 10.1248/bpb.b13-00845.
70. Deuel, T.F., Zhang, N., Yeh, H.J., Silos-Santiago, I., and Wang, Z.Y. (2002). Pleiotrophin: a cytokine with diverse functions and a novel signaling pathway. Arch Biochem Biophys *397*, 162-171. 10.1006/abbi.2001.2705.
71. Papadimitriou, E., Mourkogianni, E., Ntenekou, D., Christopoulou, M., Koutsioumpa, M., and Lamprou, M. (2022). On the role of pleiotrophin and its receptors in development and angiogenesis. Int J Dev Biol *66*, 115-124. 10.1387/ijdb.210122ep.
72. Kulesskaya, N., Molotkov, D., Sliepen, S., Mugantseva, E., Garcia Horsman, A., Paveliev, M., and Rauvala, H. (2021). Heparin-Binding Growth-Associated Molecule (Pleiotrophin) Affects Sensory Signaling and Selected Motor Functions in Mouse Model of Anatomically Incomplete Cervical Spinal Cord Injury. Front Neurol *12*, 738800. 10.3389/fneur.2021.738800.
73. Paveliev, M., Fenrich, K.K., Kislin, M., Kuja-Panula, J., Kulesskiy, E., Varjosalo, M., Kajander, T., Mugantseva, E., Ahonen-Bishopp, A., Khiroug, L., et al. (2016). HB-GAM (pleiotrophin) reverses inhibition of neural regeneration by the CNS extracellular matrix. Sci Rep *6*, 33916. 10.1038/srep33916.
74. Brandebura, A.N., Asbell, Q.N., Micael, M.K.B., and Allen, N.J. (2023). Dysregulation of astrocyte-secreted pleiotrophin contributes to neuronal structural and functional deficits in Down Syndrome. bioRxiv. 10.1101/2023.09.26.559633.
75. Gaiano, N., and Fishell, G. (2002). The role of notch in promoting glial and neural stem cell fates. Annu Rev Neurosci *25*, 471-490. 10.1146/annurev.neuro.25.030702.130823.
76. Grandbarbe, L., Bouissac, J., Rand, M., Hrabe de Angelis, M., Artavanis-Tsakonas, S., and Mohier, E. (2003). Delta-Notch signaling controls the generation of neurons/glia from neural stem cells in a stepwise process. Development *130*, 1391-1402. 10.1242/dev.00374.
77. Blackwood, C.A. (2019). Jagged1 is Essential for Radial Glial Maintenance in the Cortical Proliferative Zone. Neuroscience *413*, 230-238. 10.1016/j.neuroscience.2019.05.062.
78. Stogsdill, J.A., Ramirez, J., Liu, D., Kim, Y.H., Baldwin, K.T., Enustun, E., Ejikeme, T., Ji, R.R., and Eroglu, C. (2017). Astrocytic neuroligins control astrocyte morphogenesis and synaptogenesis. Nature *551*, 192-197. 10.1038/nature24638.
79. Wang, S., Bates, J., Li, X., Schanz, S., Chandler-Militello, D., Levine, C., Maherali, N., Studer, L., Hochedlinger, K., Windrem, M., and Goldman, S.A. (2013). Human iPSC-derived oligodendrocyte progenitor cells can myelinate and rescue a mouse model of congenital hypomyelination. Cell Stem Cell *12*, 252-264. 10.1016/j.stem.2012.12.002.
80. Windrem, M.S., Schanz, S.J., Guo, M., Tian, G.F., Washco, V., Stanwood, N., Rasband, M., Roy, N.S., Nedergaard, M., Havton, L.A., et al. (2008). Neonatal chimerization with human glial progenitor cells can both remyelinate and rescue the otherwise lethally hypomyelinated shiverer mouse. Cell Stem Cell *2*, 553-565. 10.1016/j.stem.2008.03.020.

81. Hasselmann, J., Coburn, M.A., England, W., Figueroa Velez, D.X., Kiani Shabestari, S., Tu, C.H., McQuade, A., Kolahdouzan, M., Echeverria, K., Claes, C., et al. (2019). Development of a Chimeric Model to Study and Manipulate Human Microglia In Vivo. Neuron. 10.1016/j.neuron.2019.07.002.
82. Svoboda, D.S., Barrasa, M.I., Shu, J., Rietjens, R., Zhang, S., Mitalipova, M., Berube, P., Fu, D., Shultz, L.D., Bell, G.W., and Jaenisch, R. (2019). Human iPSC-derived microglia assume a primary microglia-like state after transplantation into the neonatal mouse brain. Proc Natl Acad Sci U S A *116*, 25293-25303. 10.1073/pnas.1913541116.
83. Mancuso, R., Van Den Daele, J., Fattorelli, N., Wolfs, L., Balusu, S., Burton, O., Liston, A., Sierksma, A., Fourne, Y., Poovathingal, S., et al. (2019). Stem-cell-derived human microglia transplanted in mouse brain to study human disease. Nat Neurosci *22*, 2111-2116. 10.1038/s41593-019-0525-x.
84. Kim, J.Y., Pleasure, S.J., and Paredes, M.F. (2022). Cell Migration in the Mammalian Cortex. In Neuroscience in the 21st Century: From Basic to Clinical, D.W. Pfaff, N.D. Volkow, and J.L. Rubenstein, eds. (Springer International Publishing), pp. 465-482. 10.1007/978-3-030-88832-9_191.
85. Espuny-Camacho, I., Arranz, A.M., Fiers, M., Snellinx, A., Ando, K., Munck, S., Bonnefont, J., Lambot, L., Corthout, N., Omodho, L., et al. (2017). Hallmarks of Alzheimer's Disease in Stem-Cell-Derived Human Neurons Transplanted into Mouse Brain. Neuron *93*, 1066-1081 e1068. 10.1016/j.neuron.2017.02.001.
86. Chen, C., Kim, W.-Y., and Jiang, P. (2016). Humanized neuronal chimeric mouse brain generated by neonatally engrafted human iPSC-derived primitive neural progenitor cells. JCI Insight *1*. 10.1172/jci.insight.88632.
87. <nbt.4127.pdf>. 10.1038/nbt.4127©.
88. Mathews, S., Branch Woods, A., Katano, I., Makarov, E., Thomas, M.B., Gendelman, H.E., Poluektova, L.Y., Ito, M., and Gorantla, S. (2019). Human Interleukin-34 facilitates microglia-like cell differentiation and persistent HIV-1 infection in humanized mice. Mol Neurodegener *14*, 12. 10.1186/s13024-019-0311-y.
89. Trevino, A.E., Müller, F., Andersen, J., Sundaram, L., Kathiria, A., Shcherbina, A., Farh, K., Chang, H.Y., Pa□ca, A.M., Kundaje, A., et al. (2021). Chromatin and gene-regulatory dynamics of the developing human cerebral cortex at single-cell resolution. Cell *184*, 5053-5069.e5023. 10.1016/j.cell.2021.07.039.
90. Weng, Q., Wang, J., Wang, J., He, D., Cheng, Z., Zhang, F., Verma, R., Xu, L., Dong, X., Liao, Y., et al. (2019). Single-Cell Transcriptomics Uncovers Glial Progenitor Diversity and Cell Fate Determinants during Development and Gliomagenesis. Cell Stem Cell *24*, 707-723.e708. 10.1016/j.stem.2019.03.006.
91. Vieira, R., Mariani, J.N., Huynh, N.P.T., Stephensen, H.J.T., Solly, R., Tate, A., Schanz, S., Cotrupi, N., Mousaei, M., Sporring, J., et al. (2023). Young glial progenitor cells competitively replace aged and diseased human glia in the adult chimeric mouse brain. Nat Biotechnol. 10.1038/s41587-023-01798-5.
92. Hu, B.Y., Du, Z.W., Li, X.J., Ayala, M., and Zhang, S.C. (2009). Human oligodendrocytes from embryonic stem cells: conserved SHH signaling networks and divergent FGF effects. Development *136*, 1443-1452. 10.1242/dev.029447.
93. Khandker, L., Jeffries, M.A., Chang, Y.-J., Mather, M.L., Evangelou, A.V., Bourne, J.N., Tafreshi, A.K., Ornelas, I.M., Bozdagi-Gunal, O., Macklin, W.B., and Wood, T.L. (2022). Cholesterol biosynthesis defines oligodendrocyte precursor heterogeneity between brain and spinal cord. Cell reports *38*. 10.1016/j.celrep.2022.110423.
94. Foerster, S., Floriddia, E.M., van Bruggen, D., Kukanja, P., Hervé, B., Cheng, S., Kim, E., Phillips, B.U., Heath, C.J., Tripathi, R.B., et al. (2024). Developmental origin of oligodendrocytes determines their function in the adult brain. Nat Neurosci. 10.1038/s41593-024-01666-8.

95. Sloan, S.A., Darmanis, S., Huber, N., Khan, T.A., Birey, F., Caneda, C., Reimer, R., Quake, S.R., Barres, B.A., and Pasca, S.P. (2017). Human Astrocyte Maturation Captured in 3D Cerebral Cortical Spheroids Derived from Pluripotent Stem Cells. Neuron *95*, 779-790 e776. 10.1016/j.neuron.2017.07.035.
96. Xu, S.B., Li, X.R., Fan, P., Li, X., Hong, Y., Han, X., Wu, S., Chu, C., Chen, Y., Xu, M., et al. (2024). Single-Cell Transcriptome Landscape and Cell Fate Decoding in Human Brain Organoids after Transplantation. Advanced Science. 10.1002/advs.202402287.
97. Mariani, J.N., Mansky, B., Madsen, P.M., Salinas, D., Kesmen, D., Huynh, N.P.T., Kuypers, N.J., Kesel, E.R., Bates, J., Payne, C., et al. (2024). Repression of developmental transcription factor networks triggers aging-associated gene expression in human glial progenitor cells. Nature Communications *15*. 10.1038/s41467-024-48118-2.
98. Voss, A.J., Lanjewar, S.N., Sampson, M.M., King, A., Hill, E.J., Sing, A., Sojka, C., Bhatia, T.N., Spangle, J.M., and Sloan, S.A. (2023). Identification of ligand–receptor pairs that drive human astrocyte development. Nat Neurosci. 10.1038/s41593-023-01375-8.
99. A Neuroligin-3 Mutation Implicated inAutism Increases Inhibitory SynapticTransmission in Mice. (2007).
100. Tabuchi, K., Blundell, J., Etherton, M.R., Hammer, R.E., Liu, X., Powell, C.M., and Sudhof, T.C. (2007). A neuroligin-3 mutation implicated in autism increases inhibitory synaptic transmission in mice. Science *318*, 71-76. 10.1126/science.1146221.
101. Zhang, Y., Sloan, S.A., Clarke, L.E., Caneda, C., Plaza, C.A., Blumenthal, P.D., Vogel, H., Steinberg, G.K., Edwards, M.S., Li, G., et al. (2016). Purification and Characterization of Progenitor and Mature Human Astrocytes Reveals Transcriptional and Functional Differences with Mouse. Neuron *89*, 37-53. 10.1016/j.neuron.2015.11.013.
102. Jamain, S., Quach, H., Betancur, C., Rastam, M., Colineaux, C., Gillberg, I.C., Soderstrom, H., Giros, B., Leboyer, M., Gillberg, C., et al. (2003). Mutations of the X-linked genes encoding neuroligins NLGN3 and NLGN4 are associated with autism. Nat Genet *34*, 27-29. 10.1038/ng1136.
103. Wang, L., Mirabella, V.R., Dai, R., Su, X., Xu, R., Jadali, A., Bernabucci, M., Singh, I., Chen, Y., Tian, J., et al. (2022). Analyses of the autism-associated neuroligin-3 R451C mutation in human neurons reveal a gain-of-function synaptic mechanism. Mol Psychiatry. 10.1038/s41380-022-01834-x.
104. Foldy, C., Malenka, R.C., and Sudhof, T.C. (2013). Autism-associated neuroligin-3 mutations commonly disrupt tonic endocannabinoid signaling. Neuron *78*, 498-509. 10.1016/j.neuron.2013.02.036.
105. Hansen, D.V., Hanson, J.E., and Sheng, M. (2018). Microglia in Alzheimer's disease. J Cell Biol *217*, 459-472. 10.1083/jcb.201709069.
106. Holtman, I.R., Skola, D., and Glass, C.K. (2017). Transcriptional control of microglia phenotypes in health and disease. J Clin Invest *127*, 3220-3229. 10.1172/JCI90604.
107. Dashinimaev, E.B., Artyuhov, A.S., Bolshakov, A.P., Vorotelyak, E.A., and Vasiliev, A.V. (2017). Neurons Derived from Induced Pluripotent Stem Cells of Patients with Down Syndrome Reproduce Early Stages of Alzheimer's Disease Type Pathology in vitro. J Alzheimers Dis *56*, 835-847. 10.3233/JAD-160945.
108. Jin, M., Ma, Z., Dang, R., Zhang, H., Kim, R., Xue, H., Pascual, J., Finkbeiner, S., Head, E., Liu, Y., and Jiang, P. (2024). A Trisomy 21-linked Hematopoietic Gene Variant in Microglia Confers Resilience in Human iPSC Models of Alzheimer's Disease. bioRxiv. 10.1101/2024.03.12.584646.
109. Parra Bravo, C., Giani, A.M., Perez, J.M., Zhao, Z., Wan, Y., Samelson, A.J., Wong, M.Y., Evangelisti, A., Cordes, E., Fan, L., et al. (2024). Human iPSC 4R tauopathy model uncovers modifiers of tau propagation. Cell. 10.1016/j.cell.2024.03.015.

110. Jin, M., Alam, M.M., Liu, A.Y., and Jiang, P. (2022). Rag2(-/-) accelerates lipofuscin accumulation in the brain: Implications for human stem cell brain transplantation studies. Stem Cell Reports. 10.1016/j.stemcr.2022.09.012.
111. Jin, M., Ma, Z., Jiang, P. (2022). Generation of iPSC-based Human-mouse Microglial Brain Chimeras to Study Senescence of Human Microglia Cell STAR Protocols In press.
112. Dobin, A., Davis, C.A., Schlesinger, F., Drenkow, J., Zaleski, C., Jha, S., Batut, P., Chaisson, M., and Gingeras, T.R. (2013). STAR: ultrafast universal RNA-seq aligner. Bioinformatics *29*, 15-21. 10.1093/bioinformatics/bts635.
113. Li, B., and Dewey, C.N. (2011). RSEM: accurate transcript quantification from RNA-Seq data with or without a reference genome. BMC Bioinformatics *12*, 323. 10.1186/1471-2105-12-323.
114. Love, M.I., Huber, W., and Anders, S. (2014). Moderated estimation of fold change and dispersion for RNA-seq data with DESeq2. Genome Biol *15*, 550. 10.1186/s13059-014-0550-8.
115. Germain, P.L., Lun, A., Garcia Meixide, C., Macnair, W., and Robinson, M.D. (2021). Doublet identification in single-cell sequencing data using scDblFinder. F1000Res *10*, 979. 10.12688/f1000research.73600.2.
116. Trapnell, C., Cacchiarelli, D., Grimsby, J., Pokharel, P., Li, S., Morse, M., Lennon, N.J., Livak, K.J., Mikkelsen, T.S., and Rinn, J.L. (2014). The dynamics and regulators of cell fate decisions are revealed by pseudotemporal ordering of single cells. Nat Biotechnol *32*, 381-386. 10.1038/nbt.2859.
117. Qiu, X., Mao, Q., Tang, Y., Wang, L., Chawla, R., Pliner, H.A., and Trapnell, C. (2017). Reversed graph embedding resolves complex single-cell trajectories. Nat Methods *14*, 979-982. 10.1038/nmeth.4402.
118. Cao, J., Spielmann, M., Qiu, X., Huang, X., Ibrahim, D.M., Hill, A.J., Zhang, F., Mundlos, S., Christiansen, L., Steemers, F.J., et al. (2019). The single-cell transcriptional landscape of mammalian organogenesis. Nature *566*, 496-502. 10.1038/s41586-019-0969-x.
119. Jin, S., Guerrero-Juarez, C.F., Zhang, L., Chang, I., Ramos, R., Kuan, C.H., Myung, P., Plikus, M.V., and Nie, Q. (2021). Inference and analysis of cell-cell communication using CellChat. Nat Commun *12*, 1088. 10.1038/s41467-021-21246-9.
120. Jin, S., Plikus, M.V., and Nie, Q. (2023). CellChat for systematic analysis of cell-cell communication from single-cell and spatially resolved transcriptomics. bioRxiv, 2023.2011.2005.565674. 10.1101/2023.11.05.565674.

Figure 1

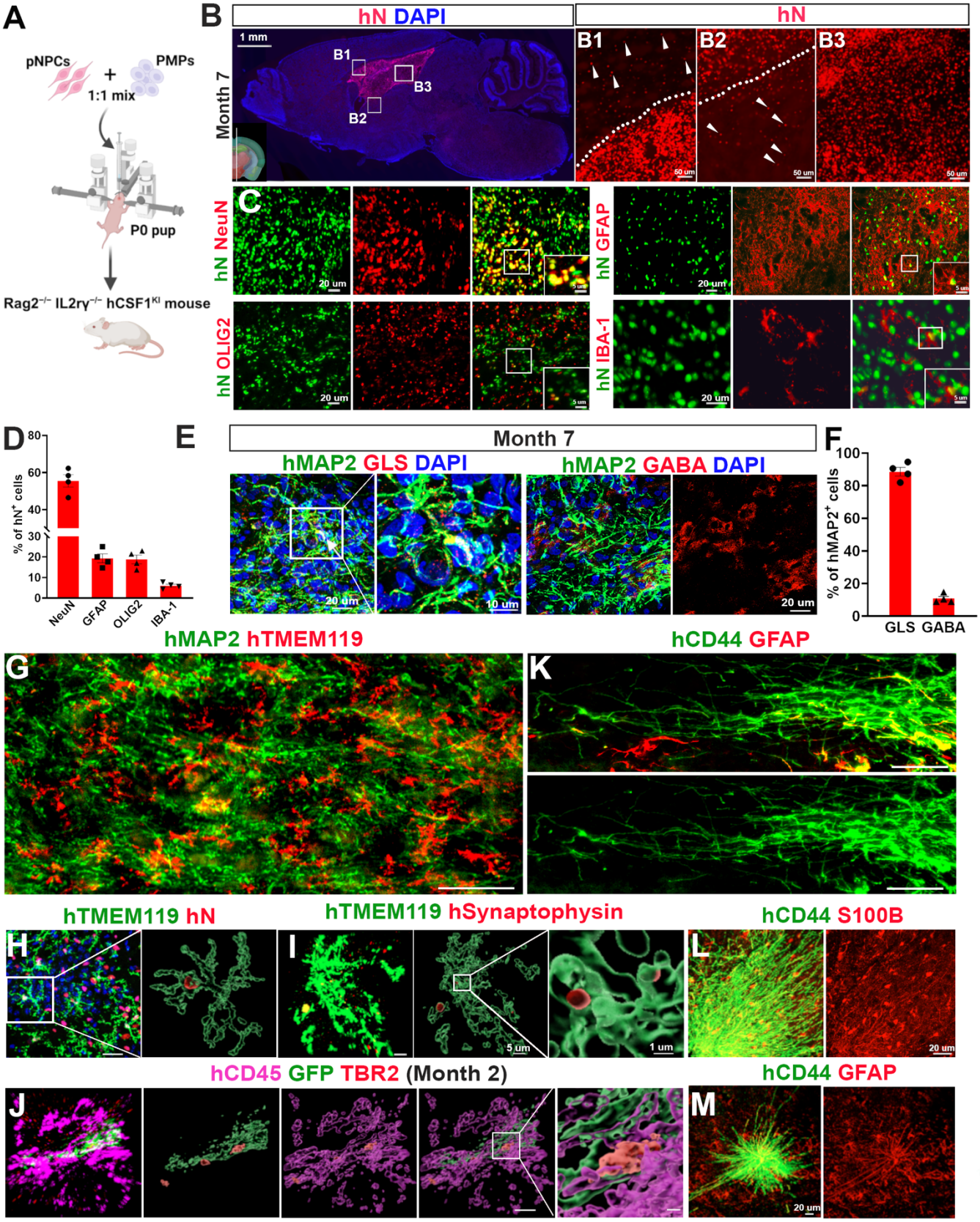
A
pNPCs
PMPs
1:1 mix
P0 pup
Rag2-/- IL2rγ-/- hCSF1KI mouse
B
hN DAPI
hN
Month 7
1 mm
B1
B2
B3
C
hN NeuN
hN GFAP
hN OLIG2
hN IBA-1
20 um
50 um
5 um
D
% of hN+ cells
NeuN
GFAP
OLIG2
IBA-1
E
Month 7
hMAP2 GLS DAPI
hMAP2 GABA DAPI
10 um
F
% of hMAP2+ cells
GLS
GABA
hMAP2 hTMEM119
G
hCD44 GFAP
K
hTMEM119 hN
H
hTMEM119 hSynaptophysin
I
hCD44 S100B
L
hCD45 GFP TBR2 (Month 2)
J
hCD44 GFAP
M

Figure 2

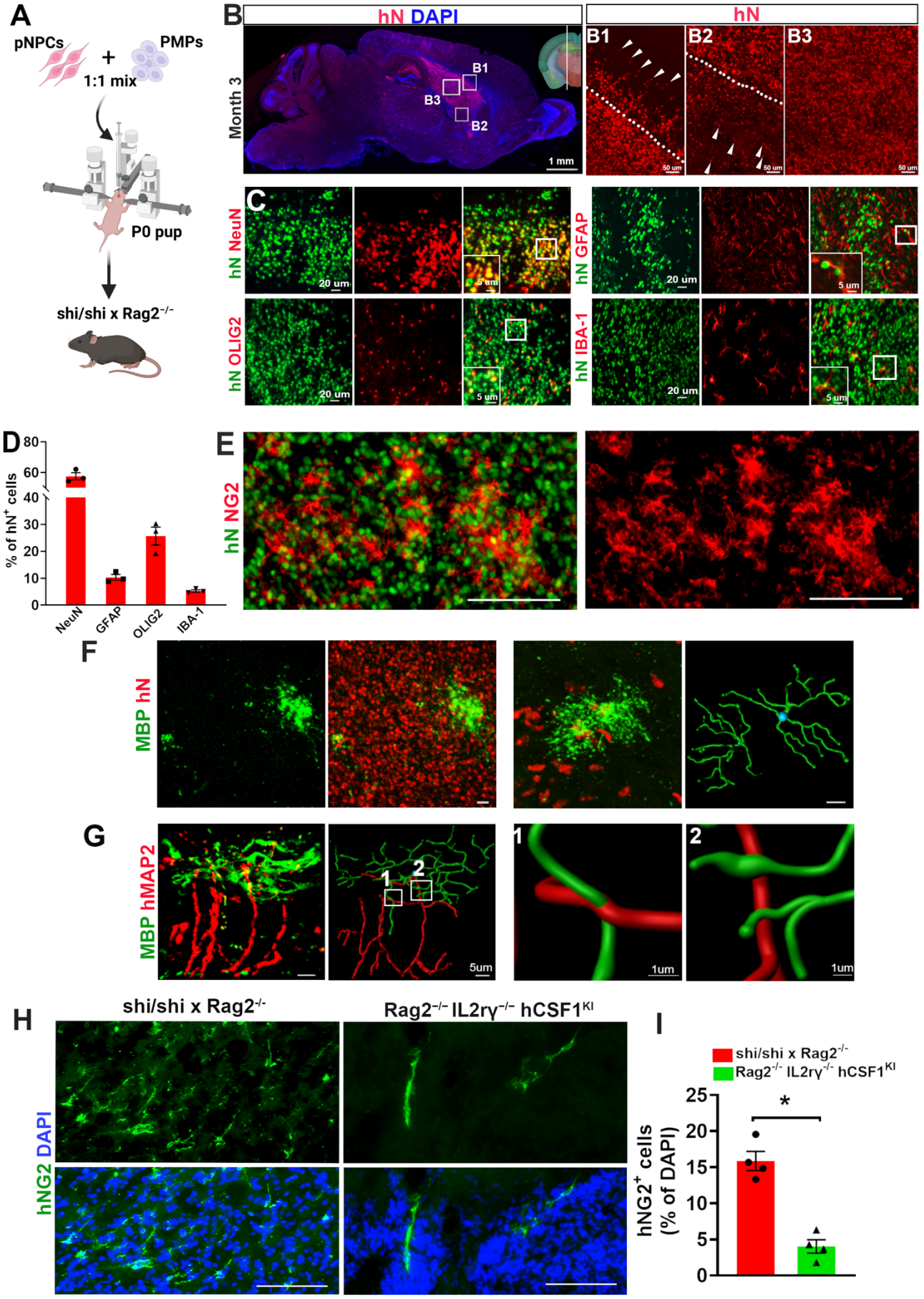
A
pNPCs
PMPs
+
1:1 mix
P0 pup
shi/shi x Rag2-/-
B
hN DAPI
hN
Month 3
B1
B2
B3
1 mm
50 um
C
hN NeuN
hN GFAP
hN OLIG2
hN IBA-1
20 um
5 um
D
% of hN+ cells
NeuN
GFAP
OLIG2
IBA-1
E
hN NG2
F
MBP hN
G
MBP hMAP2
5um
1um
H
shi/shi x Rag2-/-
Rag2-/- IL2rγ-/- hCSF1KI
hNG2 DAPI
I
shi/shi x Rag2-/-
Rag2-/- IL2rγ-/- hCSF1KI
hNG2+ cells (% of DAPI)
*

Figure 3

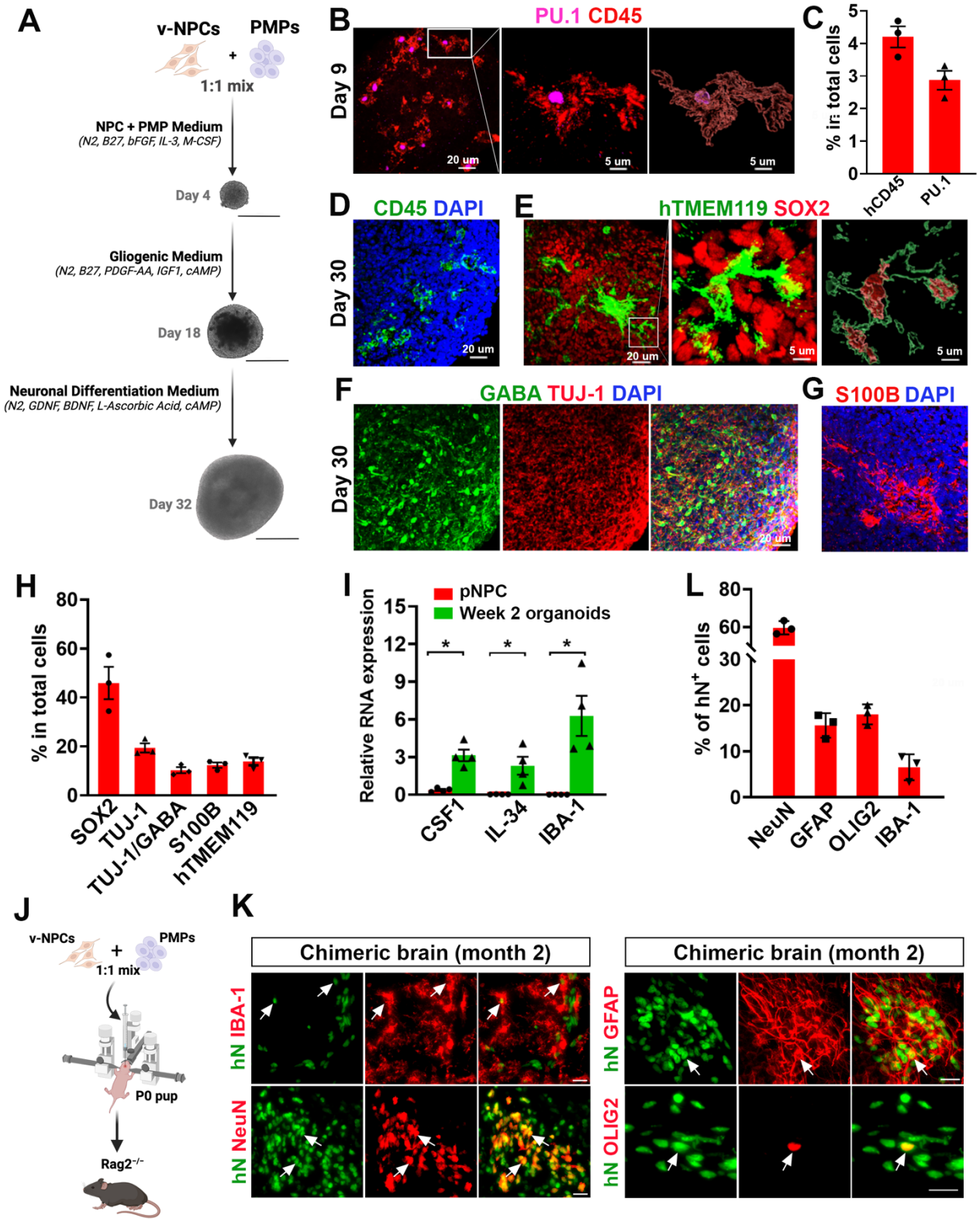
A
v-NPCs
PMPs
1:1 mix
NPC + PMP Medium
(N2, B27, bFGF, IL-3, M-CSF)
Day 4
Gliogenic Medium
(N2, B27, PDGF-AA, IGF1, cAMP)
Day 18
Neuronal Differentiation Medium
(N2, GDNF, BDNF, L-Ascorbic Acid, cAMP)
Day 32
B
PU.1 CD45
Day 9
20 um
5 um
5 um
C
% ir: total cells
hCD45
PU.1
D
CD45 DAPI
Day 30
20 um
E
hTMEM119 SOX2
20 um
5 um
5 um
F
GABA TUJ-1 DAPI
Day 30
20 um
G
S100B DAPI
H
% in total cells
SOX2
TUJ-1
TUJ-1/GABA
S100B
hTMEM119
I
pNPC
Week 2 organoids
Relative RNA expression
CSF1
IL-34
IBA-1
L
% of hN+ cells
NeuN
GFAP
OLIG2
IBA-1
J
v-NPCs
PMPs
1:1 mix
P0 pup
Rag2-/-
K
Chimeric brain (month 2)
hN IBA-1
hN NeuN
Chimeric brain (month 2)
hN GFAP
hN OLIG2

Figure 4

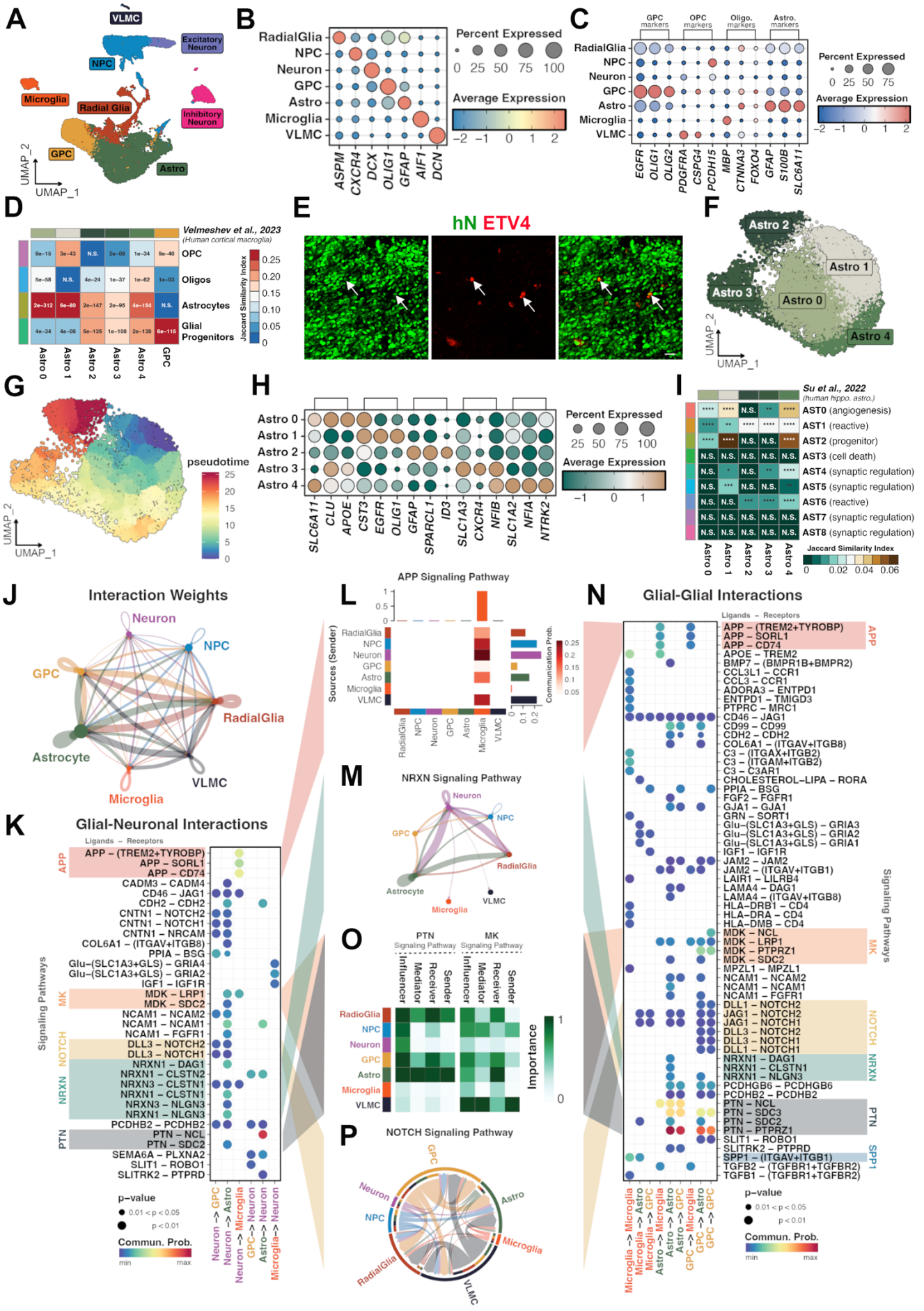
A
VLMC
Excitatory Neuron
NPC
Microglia
Radial Glia
Inhibitory Neuron
GPC
Astro
UMAP_2
UMAP_1
B
RadialGlia
NPC
Neuron
GPC
Astro
Microglia
VLMC
ASPM
CXCR4
DCX
OLIG1
GFAP
AIF1
DCN
Percent Expressed
0 25 50 75 100
Average Expression
−2 −1 0 1 2
C
GPC markers
OPC markers
Oligo. markers
Astro. markers
EGFR
OLIG1
OLIG2
PDGFRA
CSPG4
PCDH15
MBP
CTNNA3
FOXO4
GFAP
S100B
SLC6A11
D
Velmeshev et al., 2023
(Human cortical macroglia)
OPC
Oligos
Astrocytes
Glial Progenitors
Jaccard Similarity Index
Astro 0
Astro 1
Astro 2
Astro 3
Astro 4
GPC
E
hN ETV4
F
Astro 2
Astro 1
Astro 3
Astro 0
Astro 4
G
pseudotime
H
Astro 0
Astro 1
Astro 2
Astro 3
Astro 4
SLC6A11
CLU
APOE
CST3
EGFR
OLIG1
GFAP
SPARCL1
ID3
SLC1A3
CXCR4
NFIB
SLC1A2
NFIA
NTRK2
I
Su et al., 2022
(human hippo. astro.)
AST0 (angiogenesis)
AST1 (reactive)
AST2 (progenitor)
AST3 (cell death)
AST4 (synaptic regulation)
AST5 (synaptic regulation)
AST6 (reactive)
AST7 (synaptic regulation)
AST8 (synaptic regulation)
Jaccard Similarity Index
J
Interaction Weights
Neuron
NPC
GPC
RadialGlia
Astrocyte
VLMC
Microglia
K
Glial-Neuronal Interactions
Ligands – Receptors
Signaling Pathways
APP
MK
NOTCH
NRXN
PTN
p–value
Commun. Prob.
L
APP Signaling Pathway
Sources (Sender)
Communication Prob.
M
NRXN Signaling Pathway
O
PTN Signaling Pathway
MK Signaling Pathway
Influencer
Mediator
Receiver
Sender
Importance
P
NOTCH Signaling Pathway
N
Glial-Glial Interactions
Ligands – Receptors
Signaling Pathways
APP
MK
NOTCH
NRXN
PTN
SPP1
p–value
Commun. Prob.

Figure S1

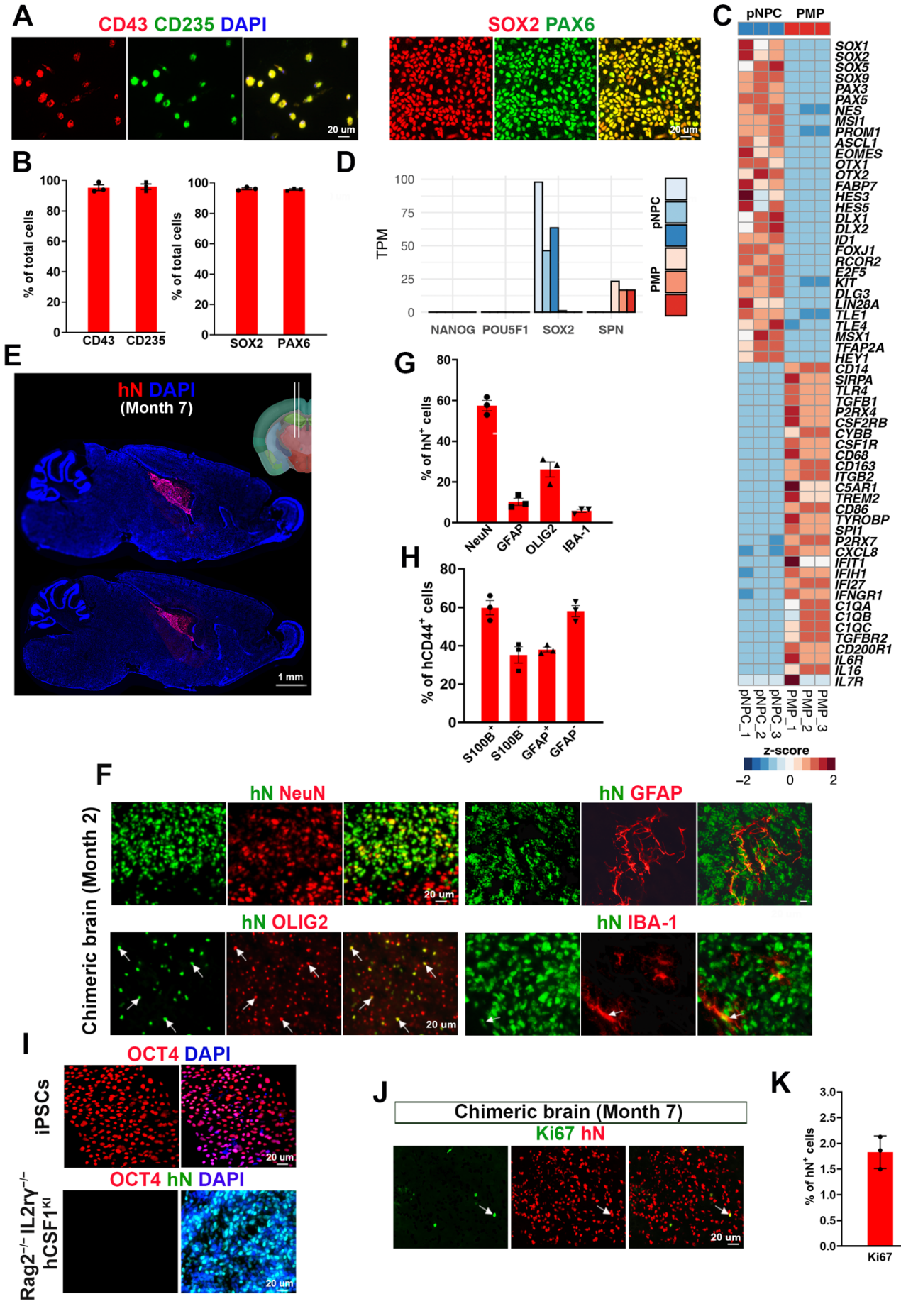
A
CD43 CD235 DAPI
20 um
SOX2 PAX6
20 um
B
% of total cells
CD43
CD235
SOX2
PAX6
D
TPM
NANOG
POU5F1
SOX2
SPN
pNPC
PMP
C
pNPC
PMP
SOX1
SOX2
SOX5
SOX9
PAX3
PAX5
NES
MSI1
PROM1
ASCL1
EOMES
OTX1
OTX2
FABP7
HES3
HES5
DLX1
DLX2
ID1
FOXJ1
RCOR2
E2F5
KIT
DLG3
LIN28A
TLE1
TLE4
MSX1
TFAP2A
HEY1
CD14
SIRPA
TLR4
TGFB1
P2RX4
CSF2RB
CYBB
CSF1R
CD68
CD163
ITGB2
C5AR1
TREM2
CD86
TYROBP
SPI1
P2RX7
CXCL8
IFIT1
IFIH1
IFI27
IFNGR1
C1QA
C1QB
C1QC
TGFBR2
CD200R1
IL6R
IL16
IL7R
pNPC_1
pNPC_2
pNPC_3
PMP_1
PMP_2
PMP_3
z-score
E
hN DAPI
(Month 7)
1 mm
G
% of hN+ cells
NeuN
GFAP
OLIG2
IBA-1
H
% of hCD44+ cells
S100B+
S100B-
GFAP+
GFAP-
F
Chimeric brain (Month 2)
hN NeuN
hN GFAP
hN OLIG2
hN IBA-1
20 um
I
iPSCs
OCT4 DAPI
Rag2-/- IL2rγ-/- hCSF1KI
OCT4 hN DAPI
20 um
J
Chimeric brain (Month 7)
Ki67 hN
20 um
K
% of hN+ cells
Ki67

Figure S2

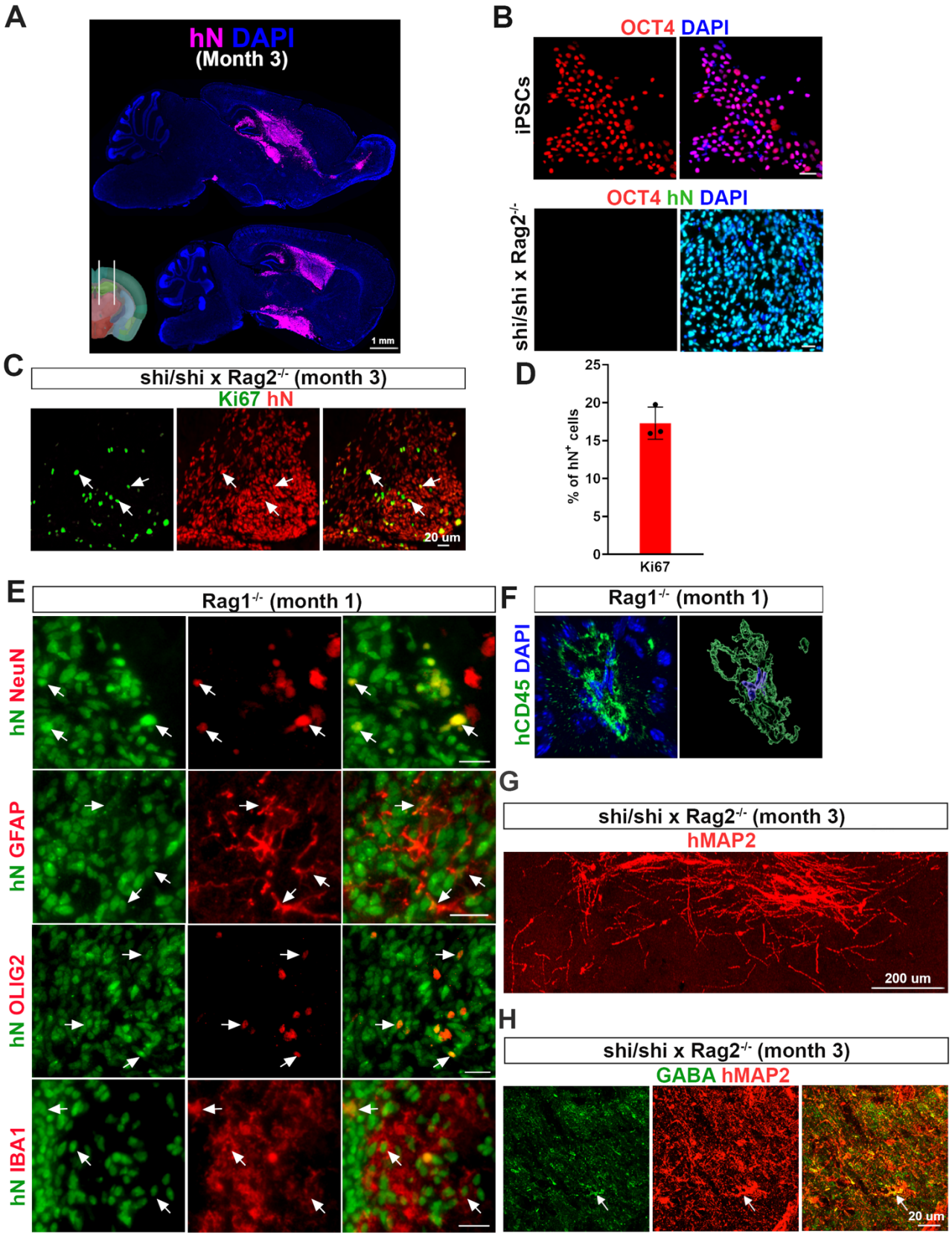
A
hN DAPI
(Month 3)
1 mm
B
OCT4 DAPI
iPSCs
OCT4 hN DAPI
shi/shi x Rag2-/-
C
shi/shi x Rag2-/- (month 3)
Ki67 hN
20 um
D
% of hN+ cells
25
20
15
10
5
0
Ki67
E
Rag1-/- (month 1)
hN NeuN
hN GFAP
hN OLIG2
hN IBA1
F
Rag1-/- (month 1)
hCD45 DAPI
G
shi/shi x Rag2-/- (month 3)
hMAP2
200 um
H
shi/shi x Rag2-/- (month 3)
GABA hMAP2
20 um

Figure S3

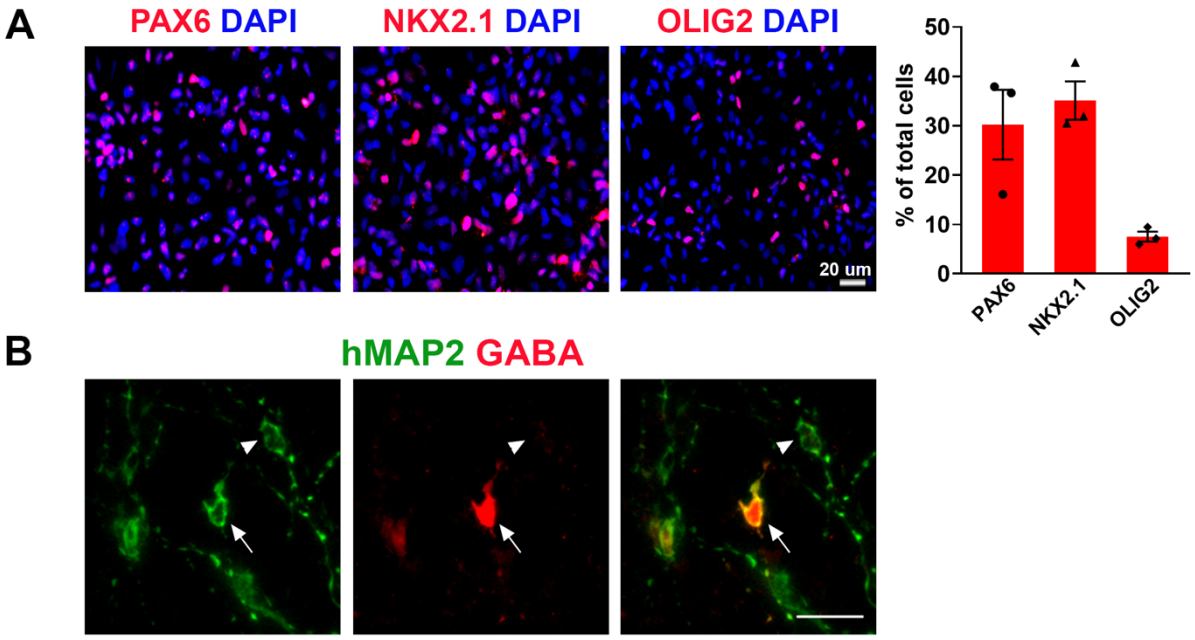
A
PAX6 DAPI
NKX2.1 DAPI
OLIG2 DAPI
20 um
% of total cells
50
40
30
20
10
0
PAX6
NKX2.1
OLIG2
B
hMAP2 GABA

Figure S4

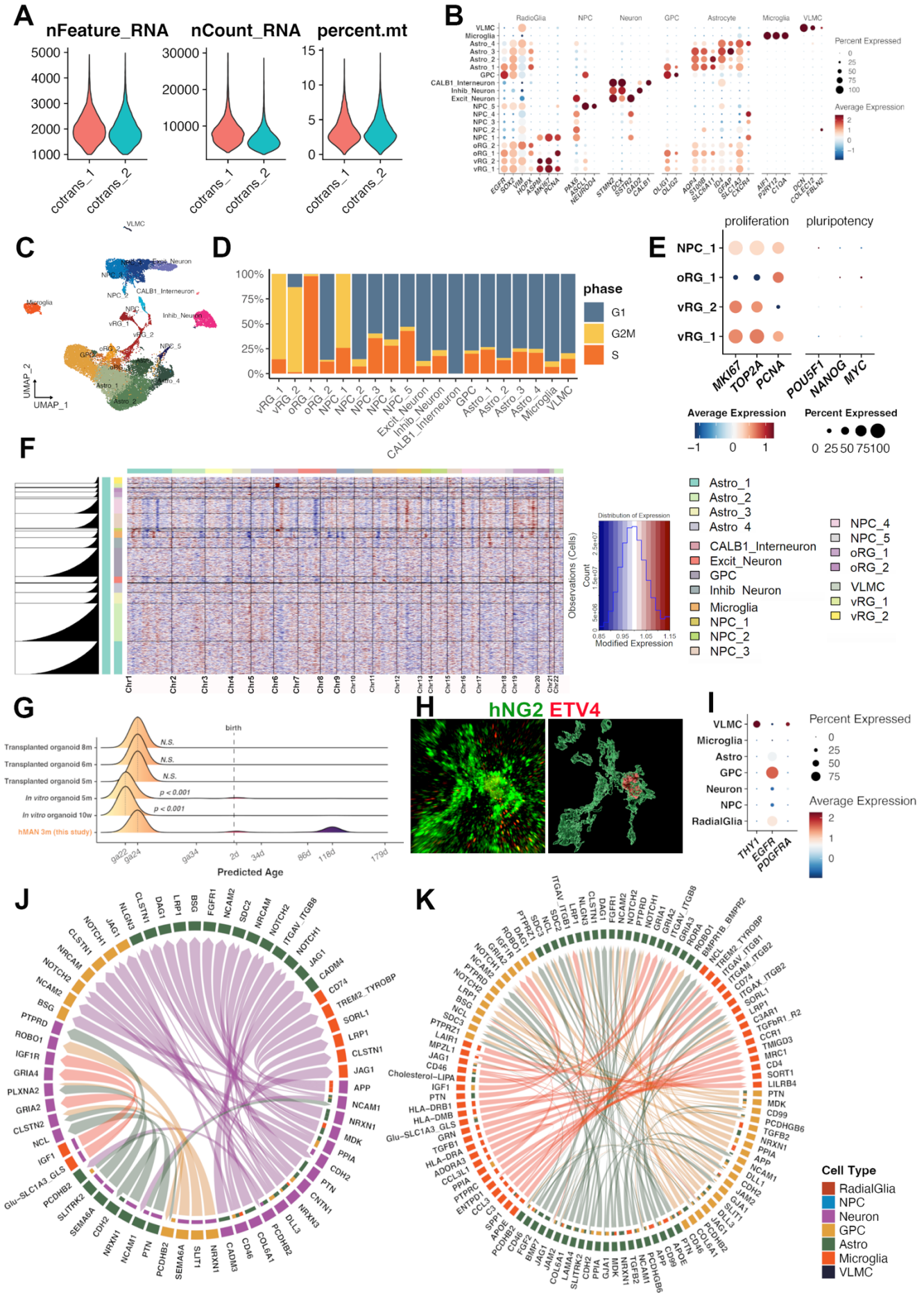
A
nFeature_RNA
nCount_RNA
percent.mt
cotrans_1
cotrans_2
B
RadioGlia
NPC
Neuron
GPC
Astrocyte
Microglia
VLMC
Percent Expressed
Average Expression
C
UMAP_1
UMAP_2
D
phase
G1
G2M
S
E
proliferation
pluripotency
NPC_1
oRG_1
vRG_2
vRG_1
MKI67
TOP2A
PCNA
POU5F1
NANOG
MYC
Average Expression
Percent Expressed
F
Observations (Cells)
Distribution of Expression
Modified Expression
Astro_1
Astro_2
Astro_3
Astro_4
CALB1_Interneuron
Excit_Neuron
GPC
Inhib_Neuron
Microglia
NPC_1
NPC_2
NPC_3
NPC_4
NPC_5
oRG_1
oRG_2
VLMC
vRG_1
vRG_2
G
birth
Transplanted organoid 8m
Transplanted organoid 6m
Transplanted organoid 5m
In vitro organoid 5m
In vitro organoid 10w
hMAN 3m (this study)
N.S.
p < 0.001
Predicted Age
H
hNG2
ETV4
I
VLMC
Microglia
Astro
GPC
Neuron
NPC
RadialGlia
THY1
EGFR
PDGFRA
Percent Expressed
Average Expression
J
K
Cell Type
RadialGlia
NPC
Neuron
GPC
Astro
Microglia
VLMC